ORAMED PROJECT

Eye-Lens Dosimetry

A new Monte Carlo approach to define the operational quantity Hp(3)

F. MARIOTTI, G. GUALDRINI

ENEA - Dipartimento Biotecnologie, Agroindustria e Protezione della Salute
Centro Ricerche “E. Clementel”, Bologna

RT/2009/1/BAS

ENTE PER LE NUOVE TECNOLOGIE,
L'ENERGIA E L'AMBIENTE

ORAMED PROJECT

Eye-Lens Dosimetry

A new Monte Carlo approach to define the operational quantity Hp(3)

F. MARIOTTI, G. GUALDRINI

ENEA - Dipartimento Biotecnologie, Agroindustria e Protezione della Salute
Centro Ricerche “E. Clementel”, Bologna

RT/2009/1/BAS

The present Report is supported by the ORAMED Contract (FP7 Grant Agreement 211361 started on February 1st 2008).

EYE LENS DOSIMETRY

A new Monte Carlo approach to define the operational quantity Hp(3)

F. MARIOTTI, G. GUALDRINI

Summary

The European Union is funding the ORAMED Contract (Optimization of RAdiation protection for MEDical staff) project which aims at developing methodologies for better assessing and reducing exposures to medical staff for procedures resulting to potentially large doses or complex radiation fields, such as interventional radiology, nuclear medicine and new developments.

One of the ORAMED Working Tasks (WP2) is addressed to the discussion and implementation in the radiation protection practice of the eye lens dose equivalent.

Hp(3)ka conversion coefficients were evaluated at the GSF (German National Research Centre for Environment and Health) laboratory, employing Monte Carlo simulations an a 30 x 30 x 15 cm^3 4-elements ICRU slab phantom for various energies and angles.

The same slab is suggested by ISO 12974 for calibrating personal dosemeters in terms of $H_p(3)$.

The dosimetric assessment in terms of this quantity is seldom performed in the various workplaces (e.g. hospitals) and therefore a question rises about its usefulness and practical implementation.

The present work tries to introduce new elements in the discussion on the quantity $H_p(3)$ and to propose a more suitable theoretical cylindrical phantom (and a corresponding experimental one for the calibration procedures) to better approximate the head in which the eyes are placed.

Keywords: *$H_p(3)$, eye-lens dosimetry, H_T(eye-lens), Monte Carlo method, Air kerma backscatter factors.*

Riassunto

L'Unione Europea sta finanziando mediante il contratto ORAMED (Optimization of RAdiation protection for MEDical staff), un progetto che mira a sviluppare nuove metodologie per meglio valutare e ridurre le esposizioni del personale medico impiegato in procedure implicanti alti dosi da radiazioni, quali per esempio la radiologia interventistica e la medicina nucleare.

Uno dei compiti di tale progetto consiste nello studio ed attuazione nella pratica di radioprotezione della quantità equivalente di dose al cristallino, $H_p(3)$.

I coefficienti di conversione per $H_p(3)/ka$ sono stati valutati dal GSF (German National Research Centre for Environment and Health) di Monaco, mediante simulazioni Monte Carlo, su di un fantoccio teorico 30 x 30 x 15 cm^3 4-elementi ICRU e dall'ENEA su di un fantoccio di dimensioni ridotte 15 x 20 x 20 cm^3 4-elementi ICRU per varie energie ed angoli di incidenza.

La norma ISO 12974 suggerisce di usare il medesimo fantoccio 30 x 30 x 15 cm^3 per la calibrazione di dosimetri personali in termini di H_p (3).

La valutazione dosimetrica in termini di tale quantità è raramente eseguita nei vari luoghi di lavoro ed è quindi necessario valutarne la sua utilità.

Il presente lavoro cerca di introdurre nuovi elementi nel dibattito sulla quantità H_p (3) e di proporre un nuovo fantoccio teorico (e di uno corrispondente per il suo impiego nella calibrazione di dosimetri per $H_p(3)$) che meglio rappresenti la testa e la posizione degli occhi nella stessa.

Parole chiave: $H_p(3)$, dosimetria del cristallino, H_T(cristallino), metodo Monte Carlo, fattori di retrodiffusione

INDICE

1. INTRODUCTION

ORAMED (Optimization of RAdiation protection for MEDical staff) is a project [1] financed by the European Union 7th framework programme which aims at developing methodologies for better assessing and reducing doses to medical staff in interventional radiology and nuclear medicine.

One of the ORAMED Working Tasks (WP2) is addressed to the discussion and the implementation of the eye lens dose equivalent and to the operational quantities that better approximates it: $H_p(3)$.

The dosimetric assessment in terms of this quantity is seldom performed and therefore a question rises about its usefulness and practical implementation.
While the ORAMED project is being carried out, the new ICRP 103 Recommendations have been issued [2]. ICRP 103 contains some considerations on $H_p(3)$, implicitly considering it as a secondary importance quantity, in some way evaluated using $H_p(0.07)$.
At the same time the report shows that the relevant number of eye opacities (cataract) found in the exposed population could bring to reconsider the dose level for this kind or radiation damage. Indeed a comprehensive panoramic view of this topic was effectively outlined during the winter school on low doses held at PTB (Braunschweig, Germany) by R. Shore [3].

The aim of WP2 is to develop a personal dosemeter characterized in term of $H_p(3)$. Until now $H_p(3)$ conversion coefficients were not reported in the official recommendations and the available data were calculated for a 30 x 30 x 15 cm^3 slab phantom that is far away to represent the head. A reduced slab phantom, for both calculating the quantities and type testing personal dosemeter in terms of the operational quantity, was previously proposed by ENEA-IRP Bologna team. The study demonstrated that a reduced slab phantom is better representative of a real situation, but the angular dependence of $H_p(3,\alpha)$ due to the edges of the slab reduces its applicability. Therefore a better suited phantom is proposed.

The present work tries to introduce new elements in the discussion on the quantity suggesting a cylindrical theoretical phantom (and a corresponding experimental one for the calibration procedures) to better approximate the head in which the eyes are placed.

2. EYE LENS DOSIMETRY

For individual monitoring ICRU (ICRU47 [5] – ICRU51 [7]) defines the Personal Dose Equivalent $H_p(d)$.
The Personal Dose Equivalent is the dose equivalent in soft tissue below a specified point on the body at an appropriate depth *d*. It is recommended that the depth d should be expressed in mm. For weakly penetrating radiation, a depth of 0.07 mm for the skin and 3 mm for the eye lenses are employed, while for strongly penetrating radiation, a depth of 10 mm is adopted.
The quantity H_p can be measured with detectors worn on the surface of the body and covered by an appropriate thickness of tissue equivalent material and the calibration of the dosemeter should be performed under simplified conditions on an appropriate phantom.

In order to comply the theoretical definition of $H_p(d)$ at a depth *d* in the body, ICRU47 [5] and ICRU51 [7] introduced a simplified 30 x 30 x 15 cm^3 4-element ICRU slab phantom in which sets of conversion coefficients between measurable quantities and $H_p(d)$ were calculated.
For $H_p(3)$ the problem is that these coefficients are not available in the mentioned reports and can be only found, for the same simplified phantom, in a GSF Report by Till et al. [4].

Individual dosemeters have to be calibrated on phantoms providing reasonable approximation of the backscatter properties of the part of the body on which they are worn. Therefore, a set of phantoms of different shapes (i.e. cubic, cuboid or cylindrical shape) are suggested by the International Organization for Standardization (ISO) to be used for the calibration of individual dosemeters: a rod PMMA calibration phantom is required for the finger and pillar and a PMMAwater filled phantom is suggested for the wrist and ankle, whilst a 30 x 30 x 15 cm^3 water filled PMMA phantom is indicated for whole body dosemeter calibration in terms of $H_p(10)$ and $H_p(0.07)$.
The same slab is suggested by ISO 12974 [8] for calibrating personal dosemeters in terms of $H_p(3)$.

At present in practice $H_p(3)$ is estimated as a mathematical combination of the $H_p(0.07)$ and $H_p(10)$ values, but (e.g.) for nuclear medicine workers it is particularly important to evaluate directly $H_p(3)$. It has on the other hand to be pointed out that such practical rule of estimating $H_p(3)$ cannot be applied in some situations, like for electrons with energies below 2 MeV, due to the fact that the quantity Hp(10) at such energies cannot be defined as the depth of 10 mm is higher than their associated extrapolated range in soft tissue (Figure 1).

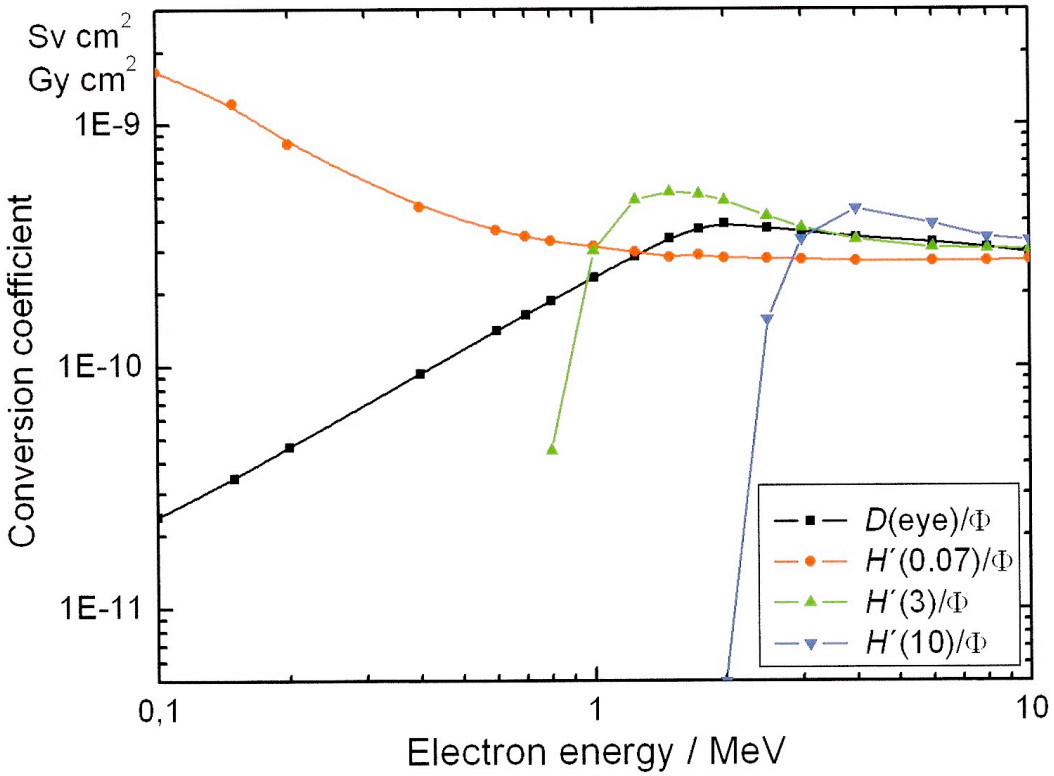

Figure 1: Electron Conversion coefficients behaviour as a function of energy. Here the quantity "directional dose equivalent" is reported, that is defined in the ICRU sphere but is well representative of $H_p(d)$. The plot demonstrates that a combination of $H_p(0,07)$ and $H_p(10)$ is not possible below E = 2 MeV.

Various groups performed a large variety of studies of depth dose distributions in slabs of different dimensions and compositions.
In particular, the problem of $H_p(3)$ was already investigated through Monte Carlo modelling and measurements in a ENEA Report by Ferrari et al. [6], introducing a 15 x 20 x 20 cm^3 cuboid phantom more representative of the head (absorption and scattering properties).

This work, based on both Monte Carlo and experimental studies, was aimed at analyzing the angular and energy test and calibration of photon personal dosemeters in terms of $H_p(3)$ on a new proposed square cylindrical phantom of ICRU tissue with 20 cm diameter and 20 cm height that can be more representative of the head than the previous phantoms.

3. MATERIALS AND METHODS

The following situation was simulated for the calculations of this study: the considered 20 cm x 20 cm square cylindrical phantom consists of ICRU tissue, that means a composition of 10.1% H, 11.1% C, 2.6% N and 76.2% O with a mass density of 1.0 $g \cdot cm^{-3}$. The surrounding medium is vacuum.
The problem was investigated through Monte Carlo modelling and measurements.
MCNP is a multipurpose Monte Carlo code developed at LANL [9] allowing to treat neutron, photon and electron transport problems in complex geometries, built relying on Boolean algebra operators and surfaces defined in the 3-D space (until 4^{th} order surfaces like torii). It is based on very updated photon and electron cross section libraries and is also provide with a large number of variance reduction techniques, available to reduce the computational uncertainty especially in cases of deep penetration calculations in the phase space.

4. AIR KERMA TO $H_p(3)$ CONVERSION COEFFICIENTS

4.1.Preliminary evaluations of Hp(3).

Before starting the calculation of the conversion coefficients in the new proposed phantom it was of interest to assess a standard way to evaluate Hp(3) bearing in mind the definition of the equivalent dose H_T(eye lens) as calculated on the anthropoid model. The eyes are a couple of organs and the conversion coefficient for the eye lens as tabulated in the international recommendations (like ICRP-74 and ICRU-57) is the average on the two eye volumes for the same irradiation. Therefore, being the cylindrical phantom assumed as a suitable substitute of the human head, a preliminary evaluation on several sensors at 3 mm depth below the phantom surface was performed with a distance between two contiguous scoring volumes equal to the intra-ocular distance as taken from the MIRD model [10]. This distance is 6 cm corresponding to an angle of 36°.
The investigation was aimed to compare the average value calculated for the two eyes and the value obtained in a volume in between them.

At the depth of 3 mm below the phantom, a set of forty scoring circular sector volumes was used to provide $H_p(3)$ (Figure 2).
The dose equivalent at specific locations in the phantom was evaluated by converting the photon fluence at the specific volumes to kerma at the same place.
The kerma in ICRU tissue at the circular scoring regions was evaluated from the photon fluence by multiplying by the photon energy (MeV) and the appropriate mass energy absorption coefficients μ_{en}/ρ for ICRU tissue.

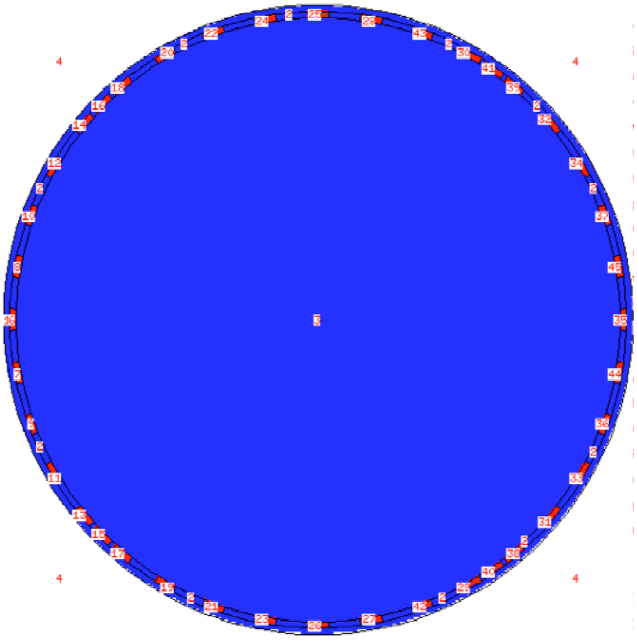

Figure 2: Schematic view of the set of forty scoring circular sector volumes used to provide $H_p(3)$.

The quantity $H_p(3)/k_a$ was compared with the data estimated by ENEA P. Ferrari et al. [6], H_T(eye lens)/k_a published in ICRU57 [3] Report and GSF Report by Till et al. [4].
In Appendix A, the complete set of the results is presented.

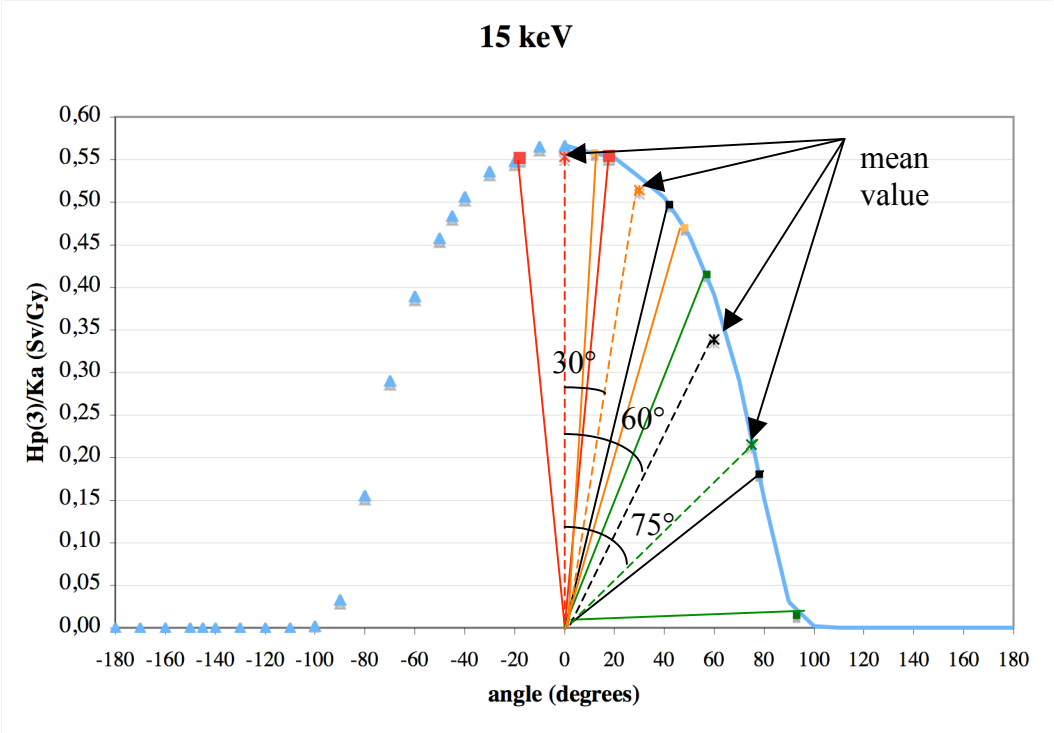

	MCNP value	Mean value	Mean value/MCNP value
0°	0,57	0,55	0,98
30°	0,53	0,51	0,97
60°	0,39	0,34	0,87
75°	0,22	0,22	0,96

Figure 3: Angular profile of H_T(eye lens)/ka for 15 keV monoenergetic radiation normally impinging on the cylindrical phantom. The plot demonstrates that the central value between the eyes well approximates the average of the two eyes equivalent dose.

The main conclusion from this study was that it is sufficient to evaluate the dose equivalent value in the central volume between the eyes as it very well approximates the average of the two eyes dose equivalents. In Figure 3 is reported the behaviour at 15 keV.

4.2.$H_p(3)/ka$ evaluations.

The Monte Carlo code MCNP-4C was employed to simulate the photon interactions within an ICRU 4-element tissue equivalent cylindrical phantom, 20 cm diameter and 20 cm height.
The data were calculated by Monte Carlo method using an ideal planar source of monoenergetic photons from 10 keV to 10 MeV, simulating an aligned and expanded field.
Two different situations have been studied:

1) The beam is normally incident on the cylinder axis (Figure 4).
2) The beam is incident with an angle of 40° on the cylinder axis (Figure 5).

The reason of the choice is to try to reproduce, besides the reference normal incidence condition, also an irradiation condition in which the operator head is placed above the irradiation source at a stated angle like in the case of interventional radiology in which (e.g.) a catheter is inserted from the femoral artery and the beam is impinging the human trunk at the level of the hearth (Fig. 6). In such a case the human trunk is acting as a scattering volume and the central forehead of the operator is seen below an angle of about 40°.

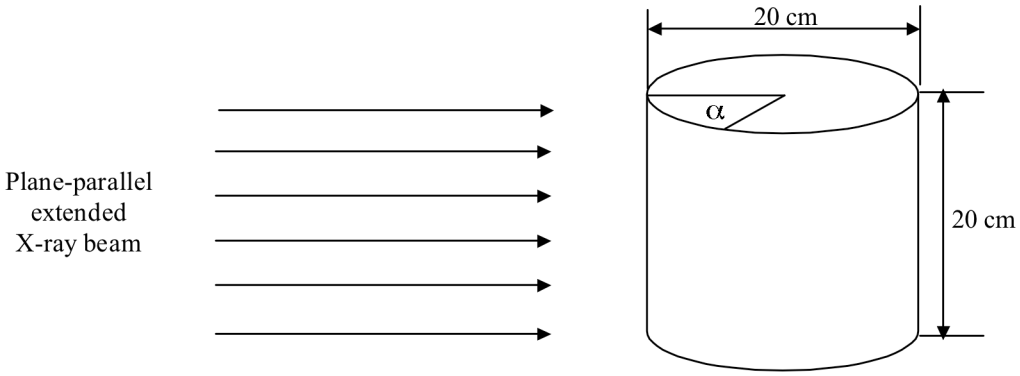

Figure 4: Schematic view of the irradiation geometry and the phantom shape with the beam normally incident on the cylinder axis.

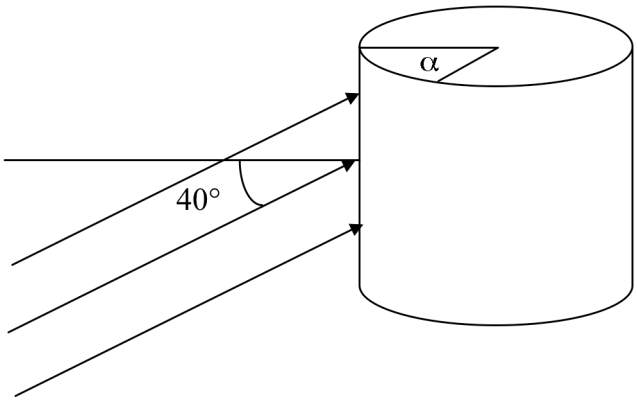

Figure 5: Schematic view of the irradiation geometry and the phantom shape with the beam incident with an angle of 40° on the cylinder axis.

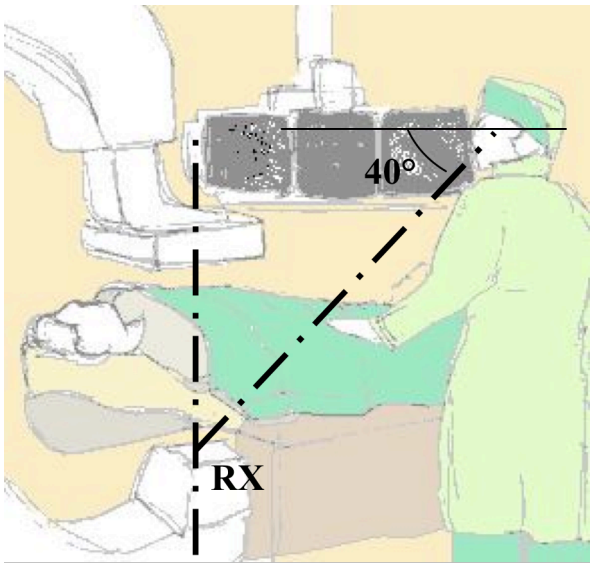

Figure 6: A typical irradiation condition of the interventional radiology in which the operator head is placed above the irradiation source at a stated angle in which (e.g.) a catheter is inserted from the femoral artery and the beam is impinging the human trunk at the level of the hearth.

A series of 23 monochromatic photon beams and 22 different incident angles were analyzed (Table 1).

Table 1: Photon beams energy and directions with respect to the normal to the incident surface of the phantom.

Energy	Angles
10, 15, 20, 30, 40, 50, 60 keV,	0°, 10°, 20°, 30°,
70, 80, 90, 100, 200 keV,	40°, 45°, 50°, 60°, 70°, 75°,
300, 400, 500, 600, 800 keV,	80°, 90°, 100°, 110°, 120°,
1, 2, 3, 6, 8, 10 MeV.	130°,140°,145°,150°,160°,170°,180°.

5. THE CALIBRATION PHANTOM: AIR KERMA BACKSCATTER FACTORS EVALUATIONS

5.1.Importance of providing suitable backscatter factor values for "nearly realistic" calibration irradiation

As it is well know, for every calibration procedure the selected phantom should be as much a possible representative of the realistic irradiation condition. Therefore a PMMA water filled cylindrical phantom of the same external dimensions of the theoretical one was developed.
For this experimental phantom a Monte Carlo model was implemented and a set of backscatter factors were calculated for the complete ISO Narrow Spectrum Series that is suggested for calibrations in the ISO guidelines [11]. In Figure 7 a picture of the investigated phantom is reported.

Figure 7: A picture of the new investigated square cylindrical phantom.

5.2.Backscatter properties study

It has also been tabulated a complete set of air kerma backscatter factors depending on the incident angle and distance from the cylindrical phantom (0 mm, 1 mm, 5 mm, 10.5 mm and 20.5 mm). In figure 8 a sketch of the model implemented in MCNP for this study is presents. A central series of belts (depending on the investigated distance) with cylindrical sector were modelled to obtain the angular values in only one run. In figure 9 an irradiation scenario is reported in 3-D geometry.
Air kerma backscatter factor (B) is defined as the ratio of the collision air kerma in presence of the phantom and the collision air kerma without the phantom.

$$B = \frac{K_a^{phantom}}{K_a}$$

For a given distance from the phantom as well as for a given incident mean energy, B is a function of the incident angle.
The set of the nine ISO Narrow-spectrum series beams was analysed at five calibration incident angles (0°, 20°, 40°, 60° and 75°) (Table 2).

Table 2: Characteristics of Narrow-spectrum Series (ISO).

Radiation quality	Tube potential (kV)	Mean energy (keV)	Additional filtration (mm)
N40	40	33	4.00 Al + 0.21 Cu
N60	60	47	4.00 Al + 0.60 Cu
N80	80	65	4.00 Al + 2.00 Cu
N100	100	83	4.00 Al + 5.00 Cu
N120	120	100	4.00 Al + 5.00 Cu + 1.00 Sn
N150	150	117	4.0 Al + 2.50 Sn
N200	200	163	4.00 Al + 2.00 Cu+ 3.00 Sn+ 1.00 Sn
N250	250	207	4.00 Al + 2.00 Sn+ 3.00 Pb
N300	300	248	4.00 Al + 3.00 Sn+5.00 Pb

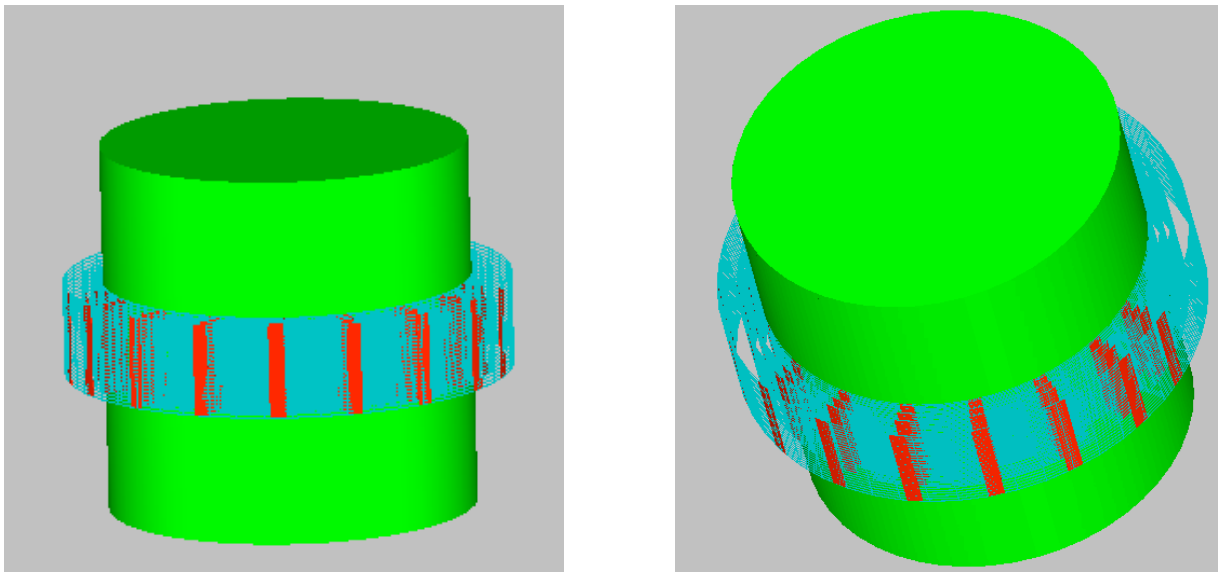

Figure 8: Sketches of the model implemented in MCNP for the backscatters properties study.

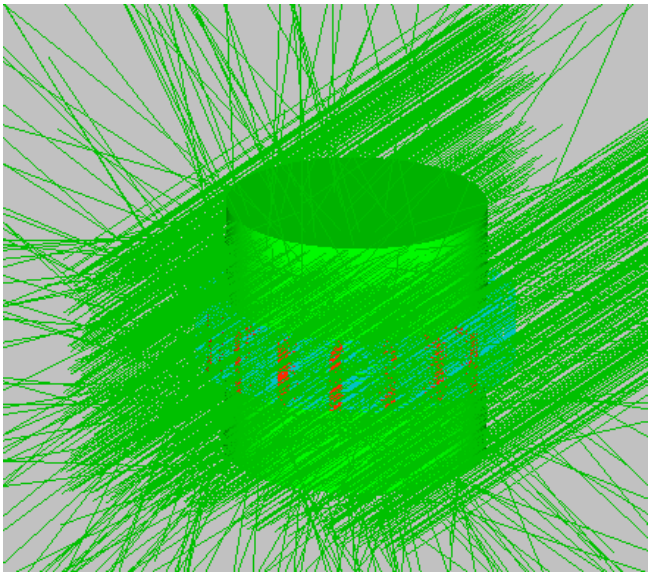

Figure 9: An irradiation scenario reported in 3-D geometry.

6. RESULTS

A detailed set of conversion coefficients for $H_p(3)$ using the new theoretical cylindrical phantom as well as the complete tabulation of the air kerma backscatter factors for all the ISO series are reported.
The plots were obtained using optimized interpolation, which could approximate the data behaviour in the most suitable way (splines etc.).
The comparison with the data from GSF Report [4] and from the former ENEA Report [6] demonstrates the significant dependence of the values on the adopted phantom.

7. CONCLUSIONS

This work presents an extensive set of conversion coefficients from air kerma to Hp(3) in a new investigated 4 element ICRU tissue equivalent square cylindrical phantom as well as selected angular dependence factors $R(E,\alpha)$. These data characterise the angular dependence of Hp(3)/ka in a tissue cylindrical phantom irradiated with monoenergetic and introduce new elements in the

discussion on the quantity proposing a more suitable theoretical phantom to better approximate the head in which the eyes are placed.
Moreover an extensive computational study has been carried out in order to determine the backscatter factors (as a function of mean energy and incident angle) for the X-ray Narrow-spectrum Series as proposed by ISO.
The cylindrical head phantom herewith proposed can be considered a better substitute of the real head and therefore the corresponding conversion coefficients and backscatter factors are reasonably more realistic.

APPENDIX A

H_T(eye lens) profiles as a function of incident angle. The colour crosses express the mean values between two eyes. Red square couple of values correspond to 0° incidence, orange 30°, black 60° and green (here absent) 75°.

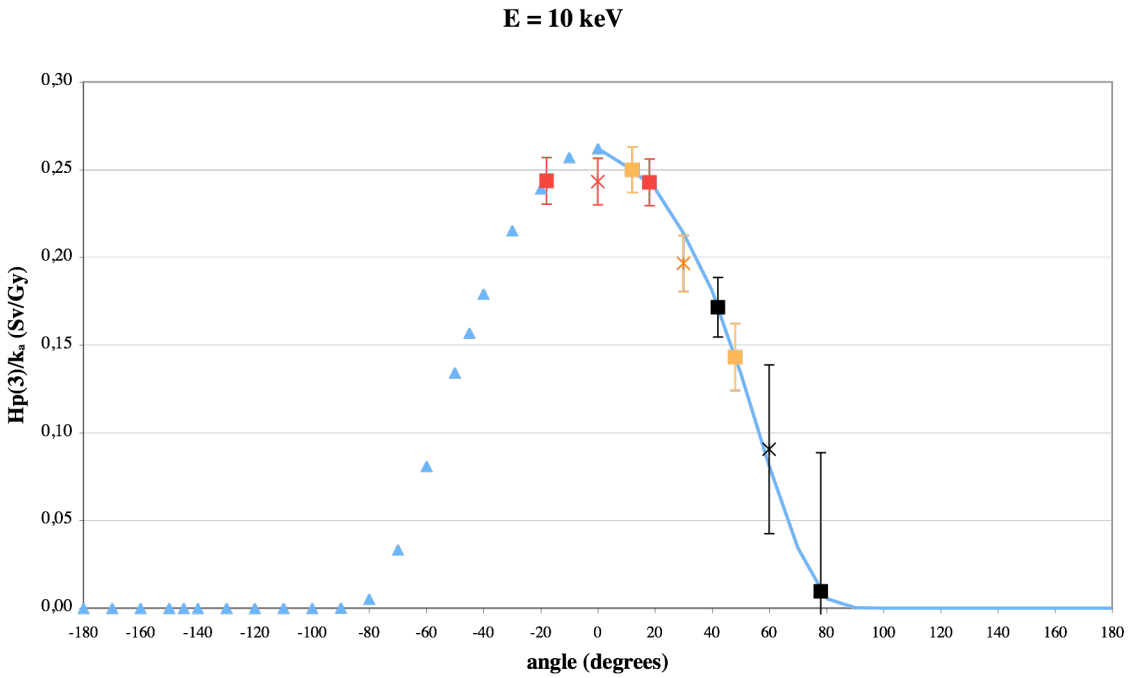

Figure A-1: $H_p(3)/k_a$ for 10 keV normally incident beam. X axis: angular scoring regions on the cylindrical phantom.

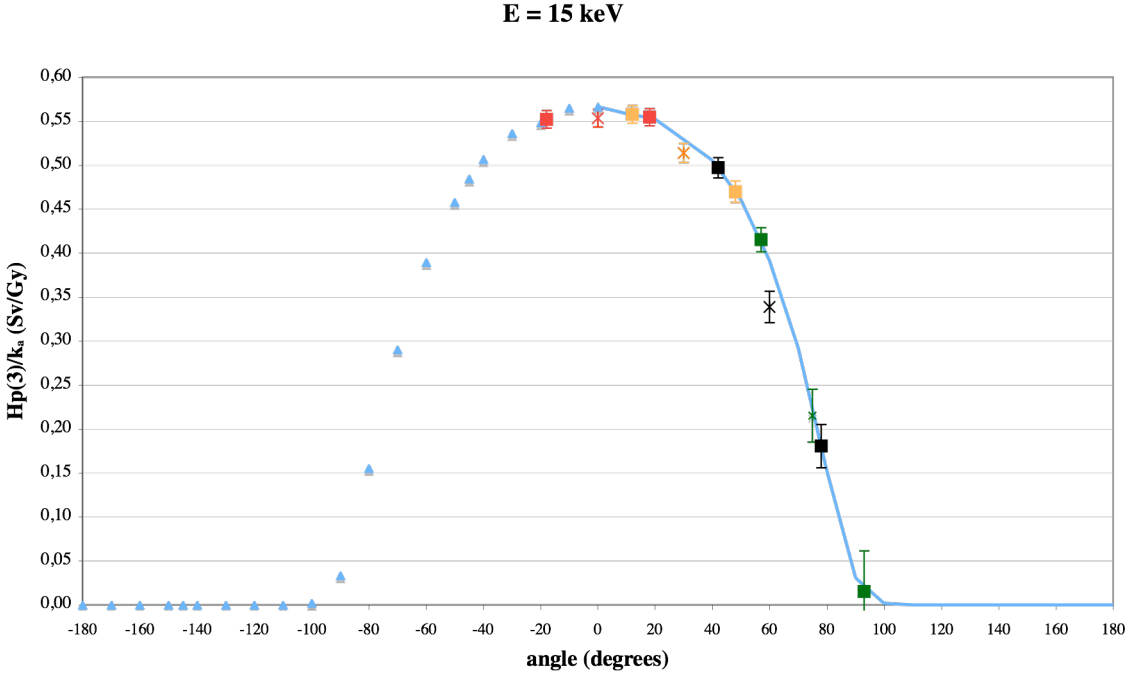

Figure A-2: $H_p(3)/k_a$ for 15 keV normally incident beam. X axis: angular scoring regions on the cylindrical phantom.

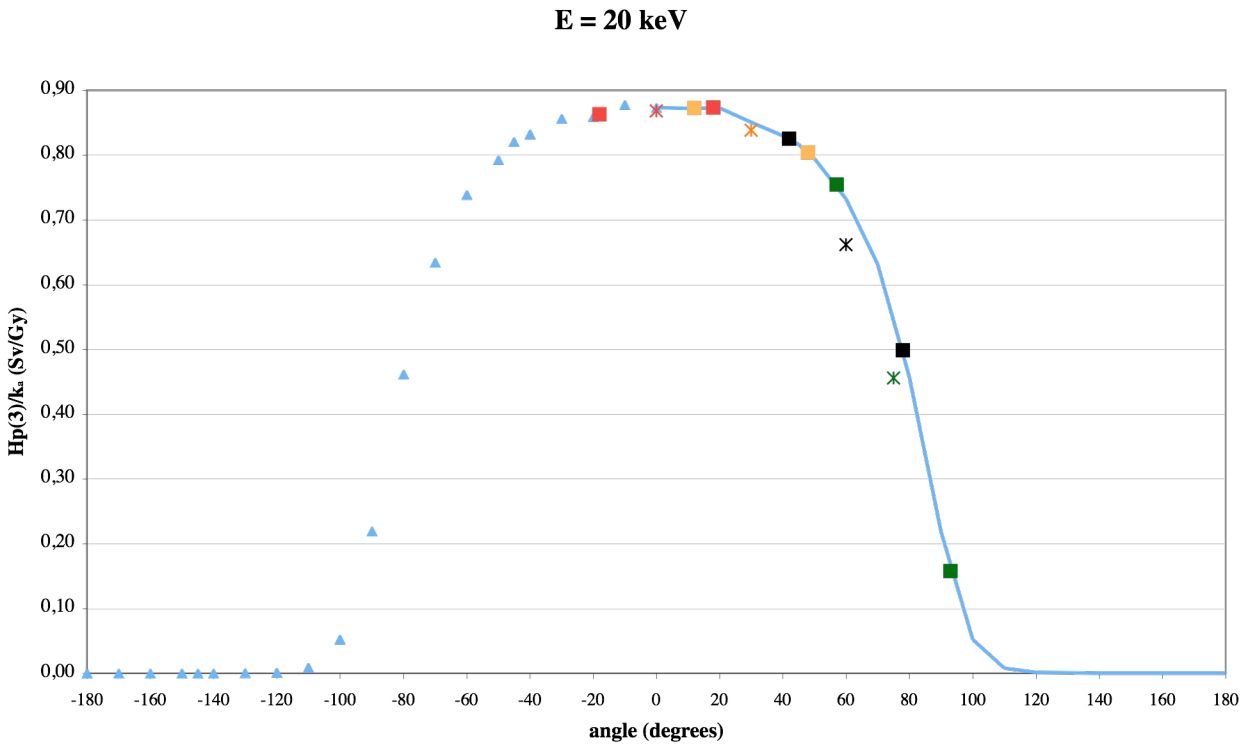

Figure A-3: $H_p(3)/k_a$ for 20 keV normally incident beam. X axis: angular scoring regions on the cylindrical phantom.

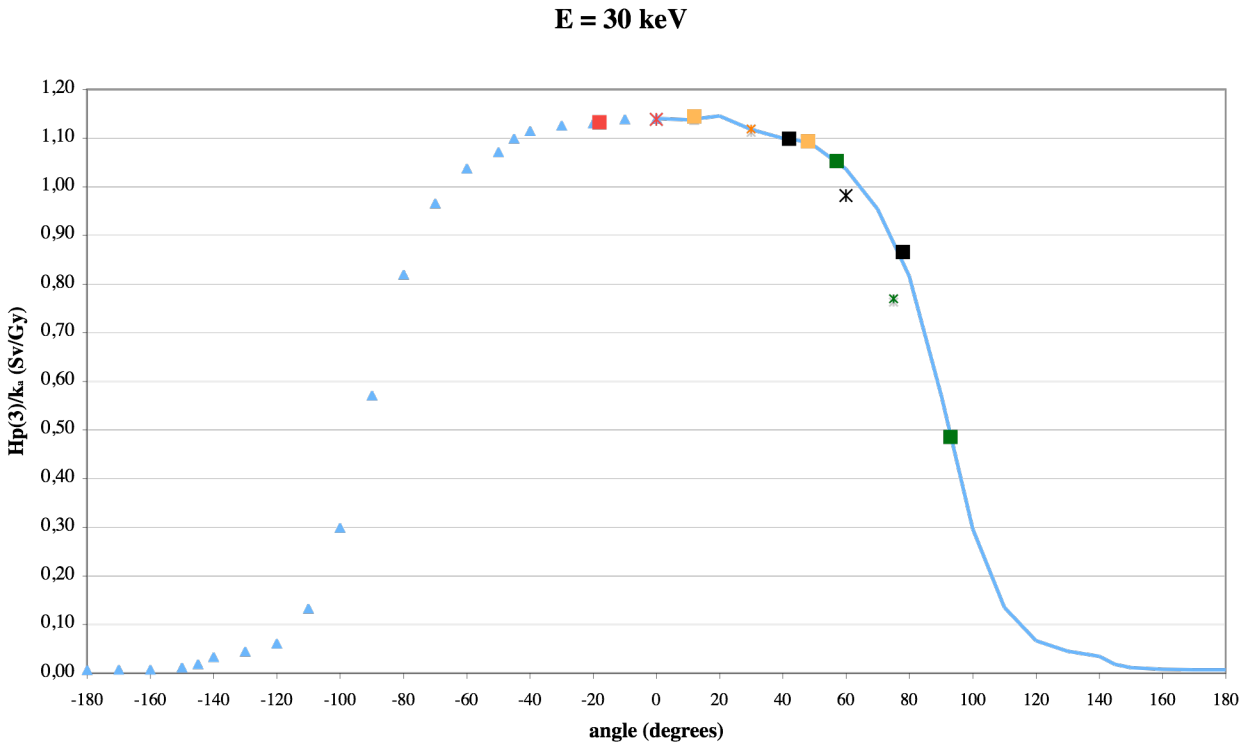

Figure A-4: $H_p(3)/k_a$ for 30 keV normally incident beam. X axis: angular scoring regions on the cylindrical phantom.

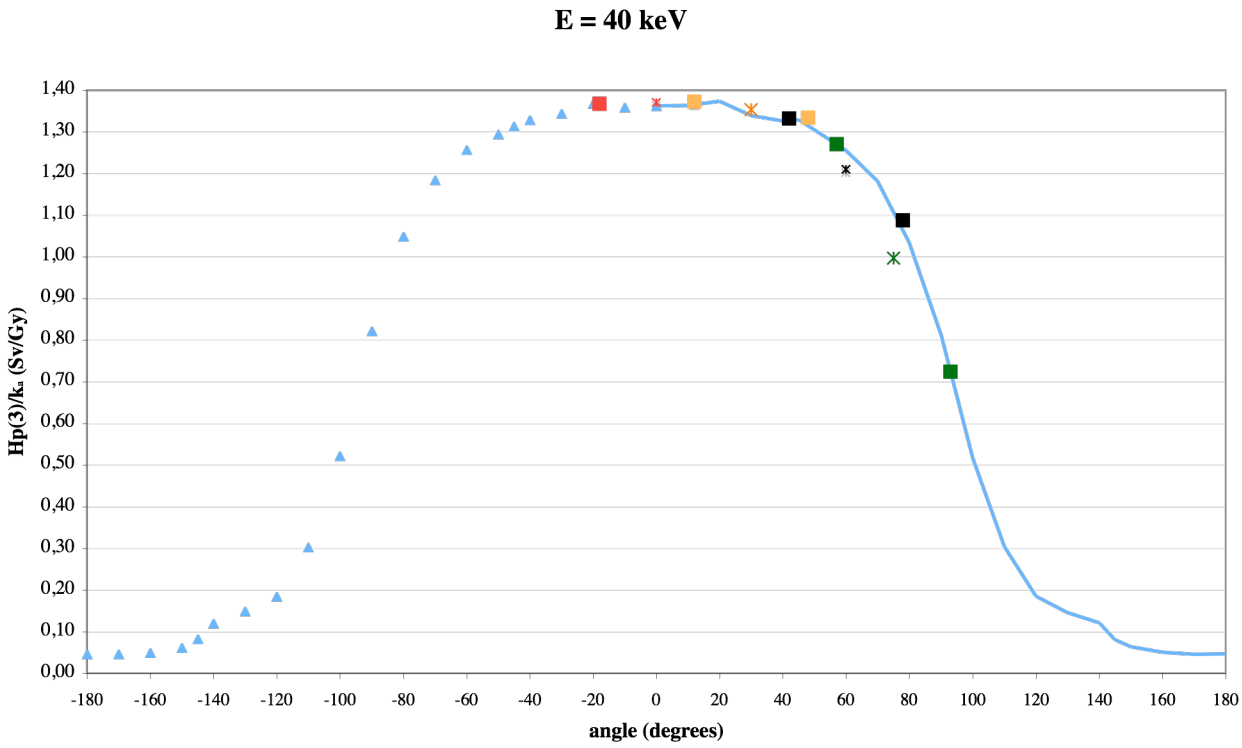

Figure A-5: $H_p(3)/k_a$ for 40 keV normally incident beam. X axis: angular scoring regions on the cylindrical phantom.

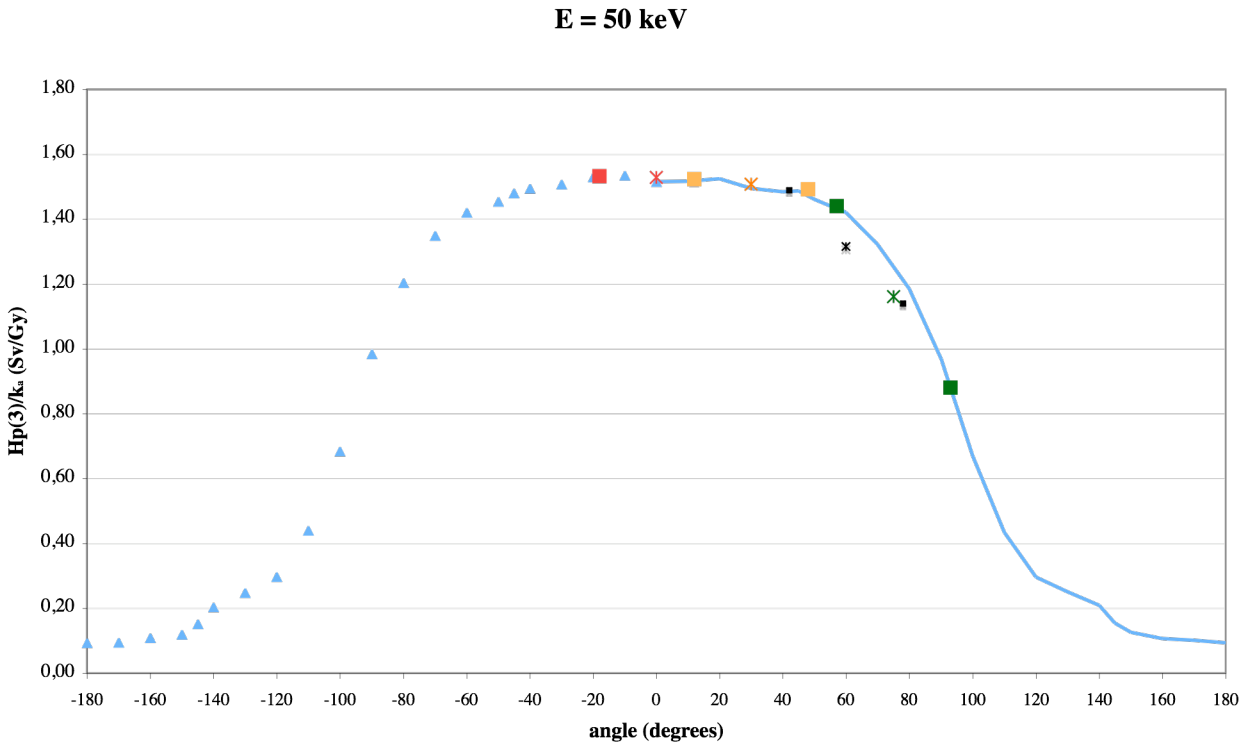

Figure A-6: $H_p(3)/k_a$ for 50 keV normally incident beam. X axis: angular scoring regions on the cylindrical phantom.

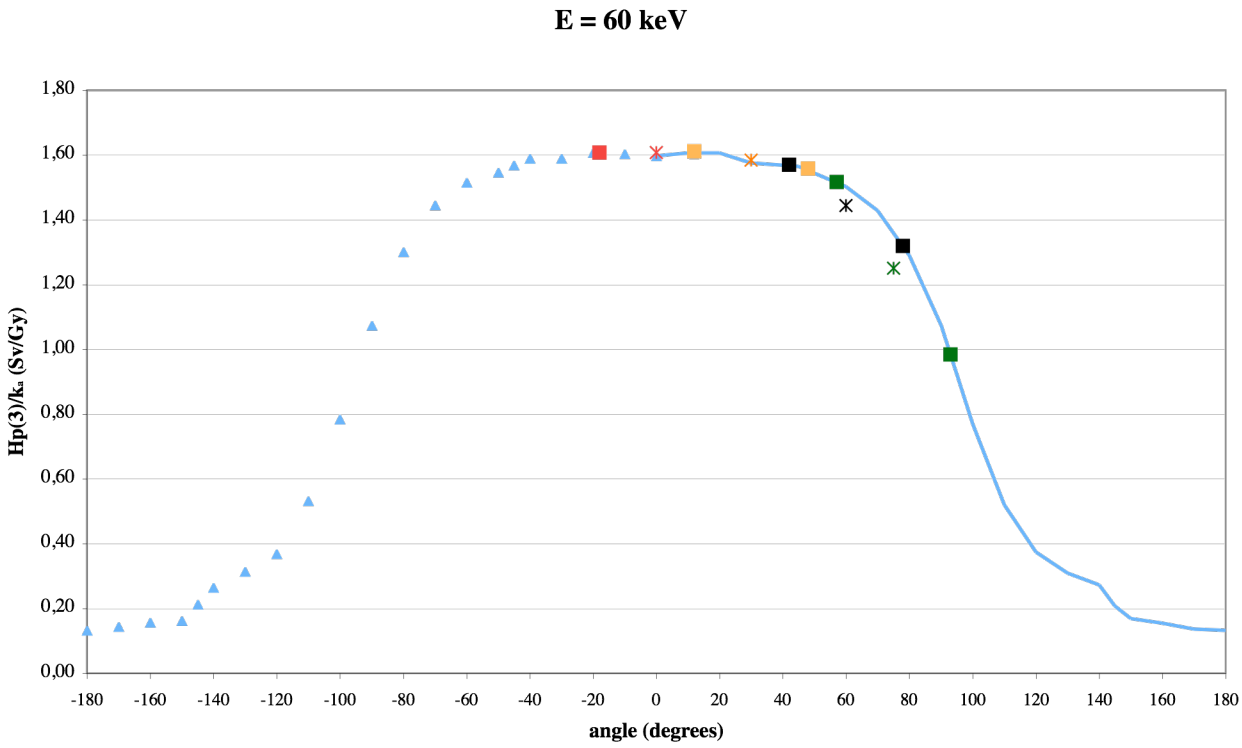

Figure A-7: $H_p(3)/k_a$ for 60 keV normally incident beam. X axis: angular scoring regions on the cylindrical phantom.

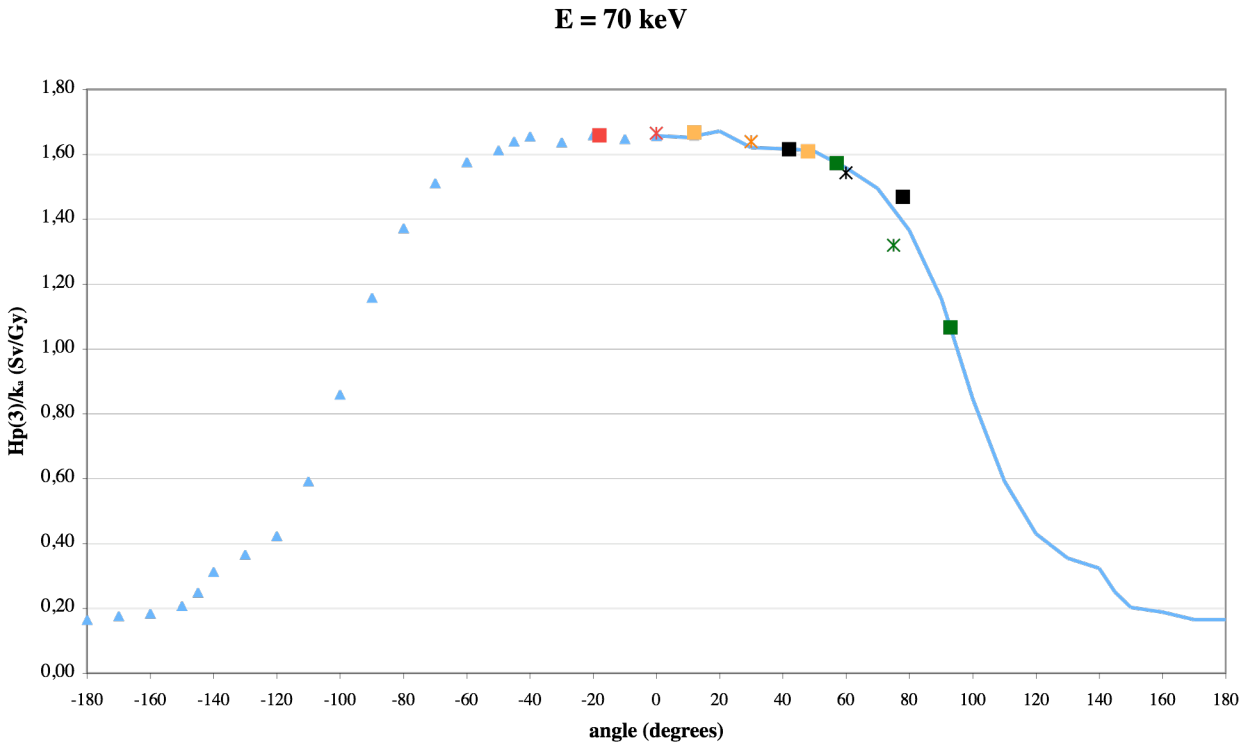

Figure A-8: $H_p(3)/k_a$ for 70 keV normally incident beam. X axis: angular scoring regions on the cylindrical phantom.

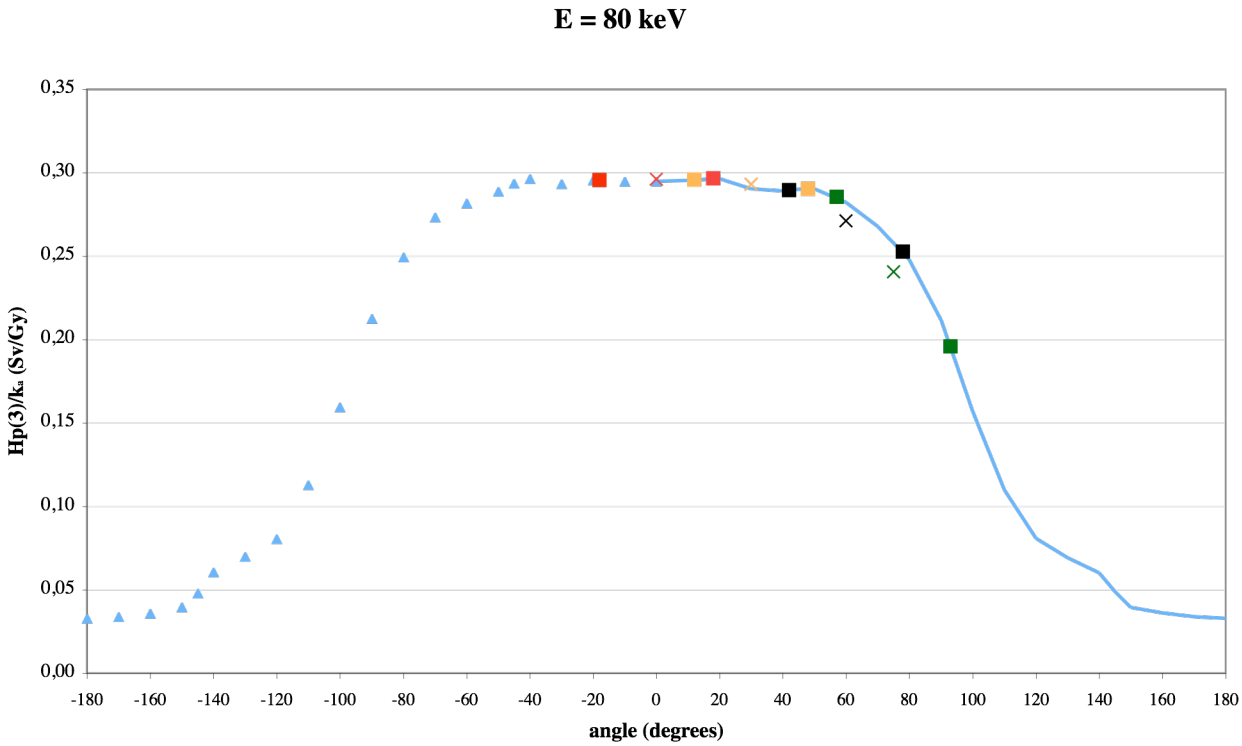

Figure A-9: $H_p(3)/k_a$ for 80 keV normally incident beam. X axis: angular scoring regions on the cylindrical phantom.

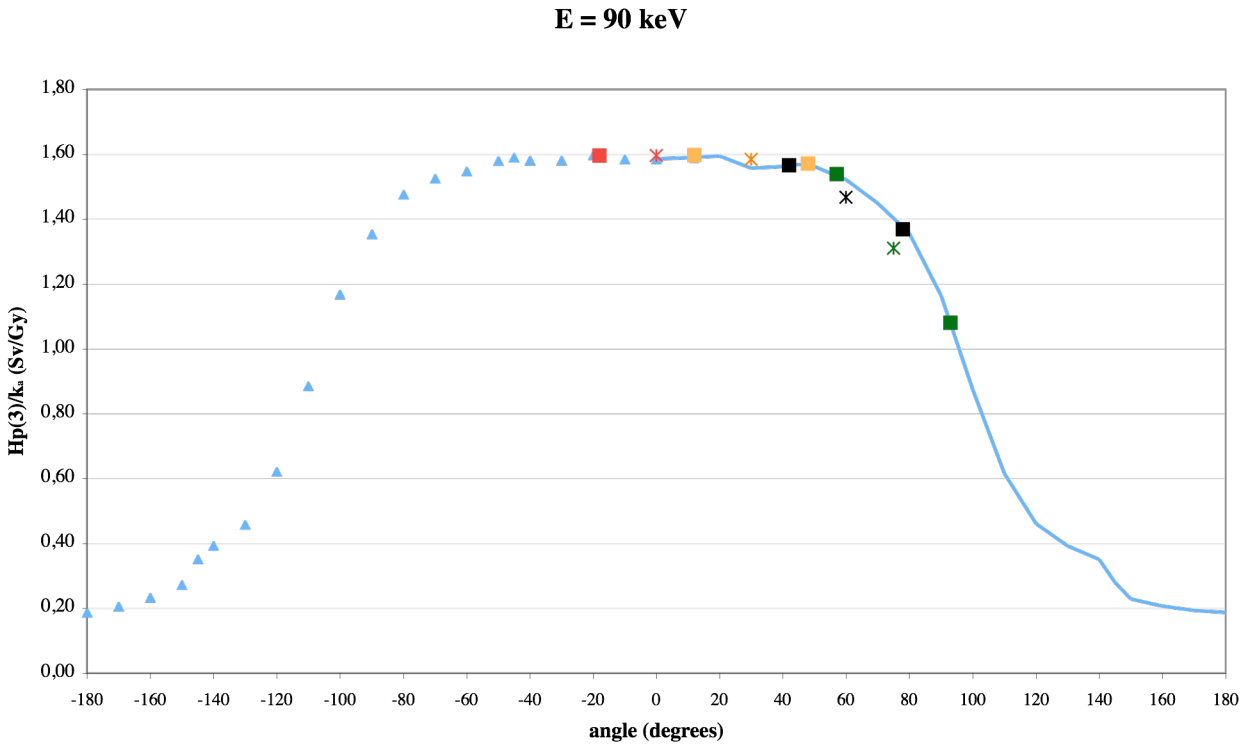

Figure A-10: $H_p(3)/k_a$ for 90 keV normally incident beam. X axis: angular scoring regions on the cylindrical phantom.

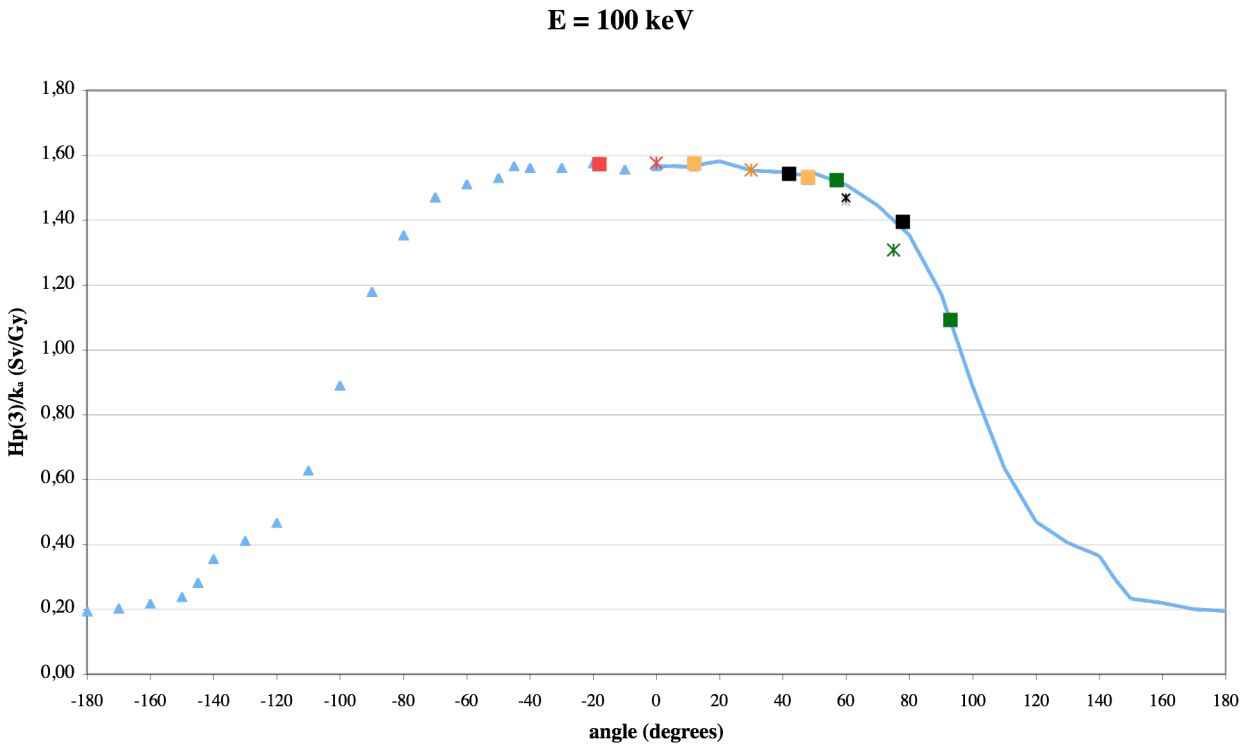

Figure A-11: $H_p(3)/k_a$ for 100 keV normally incident beam. X axis: angular scoring regions on the cylindrical phantom.

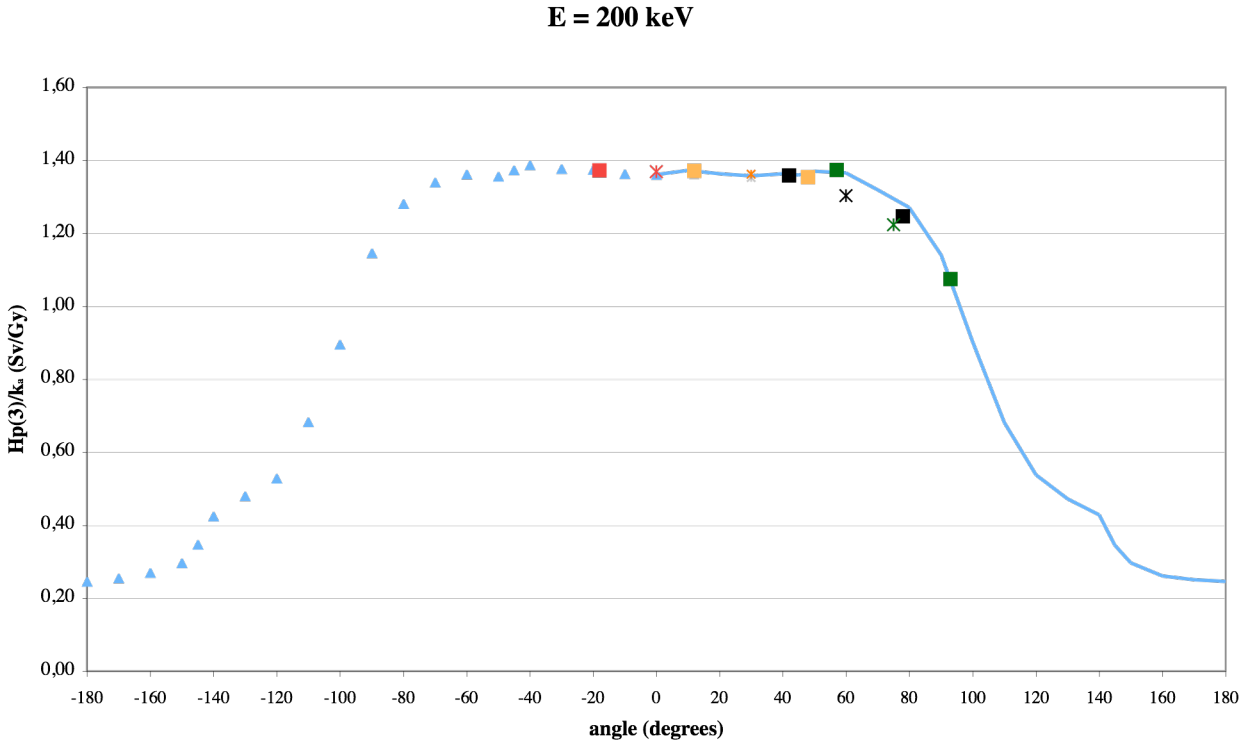

Figure A-12: $H_p(3)/k_a$ for 200 keV normally incident beam. X axis: angular scoring regions on the cylindrical phantom.

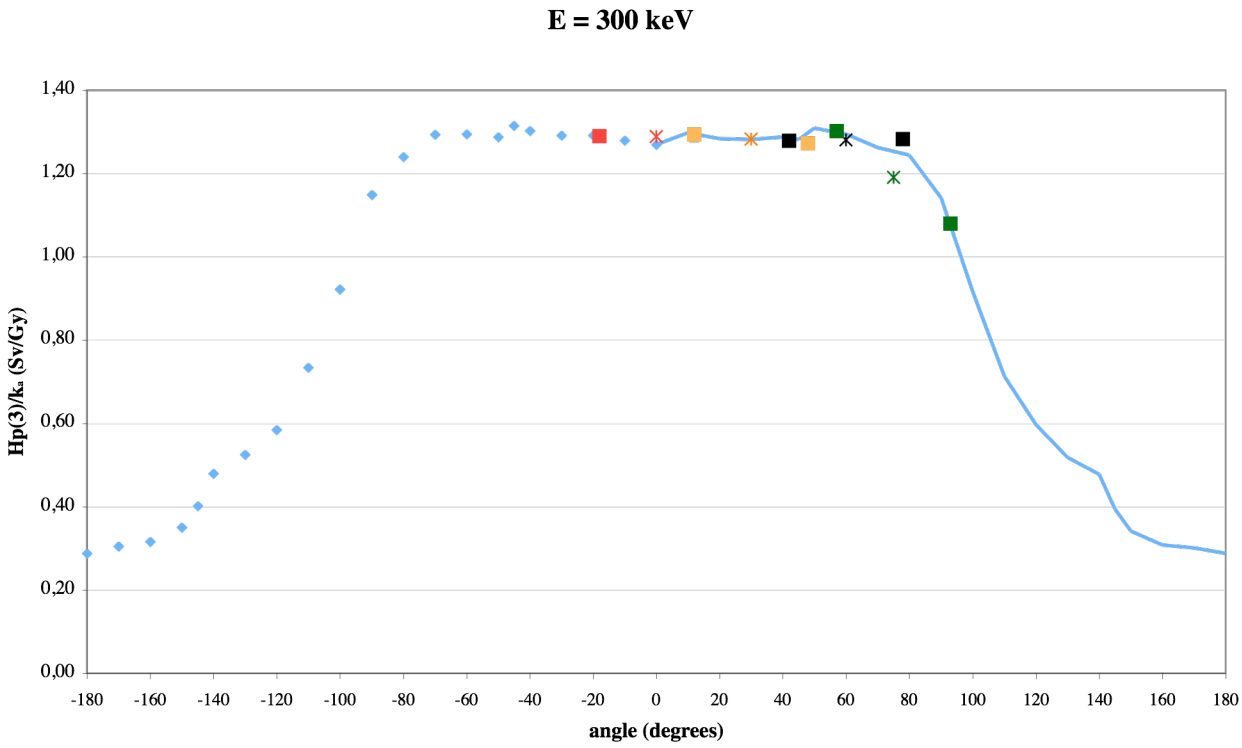

Figure A-13: $H_p(3)/k_a$ for 300 keV normally incident beam. X axis: angular scoring regions on the cylindrical phantom.

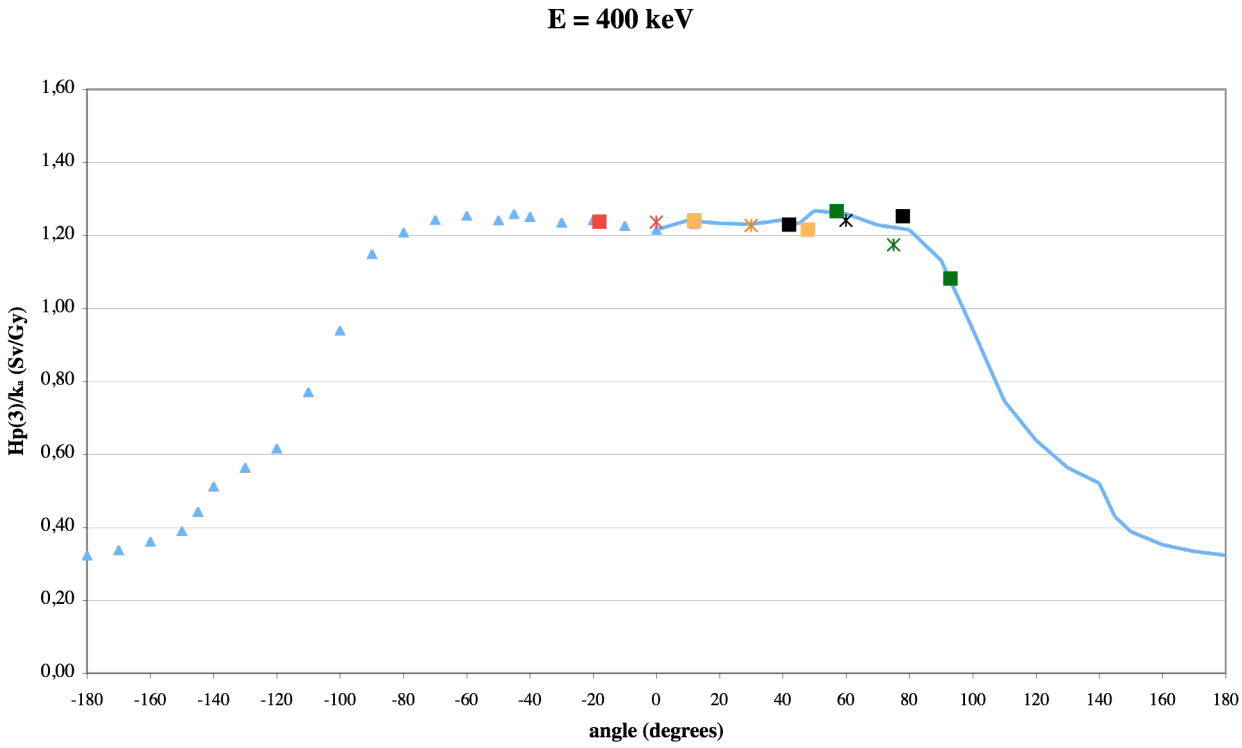

Figure A-14: $H_p(3)/k_a$ for 400 keV normally incident beam. X axis: angular scoring regions on the cylindrical phantom.

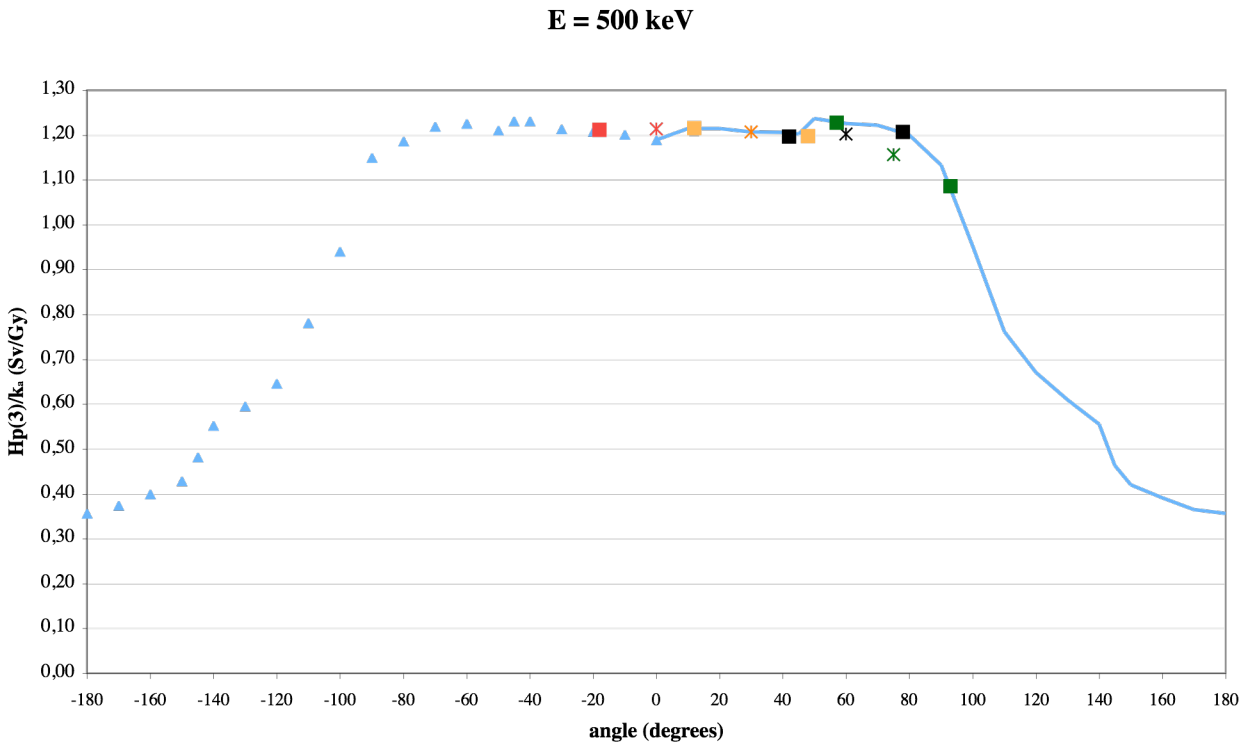

Figure A-15: $H_p(3)/k_a$ for 500 keV normally incident beam. X axis: angular scoring regions on the cylindrical phantom.

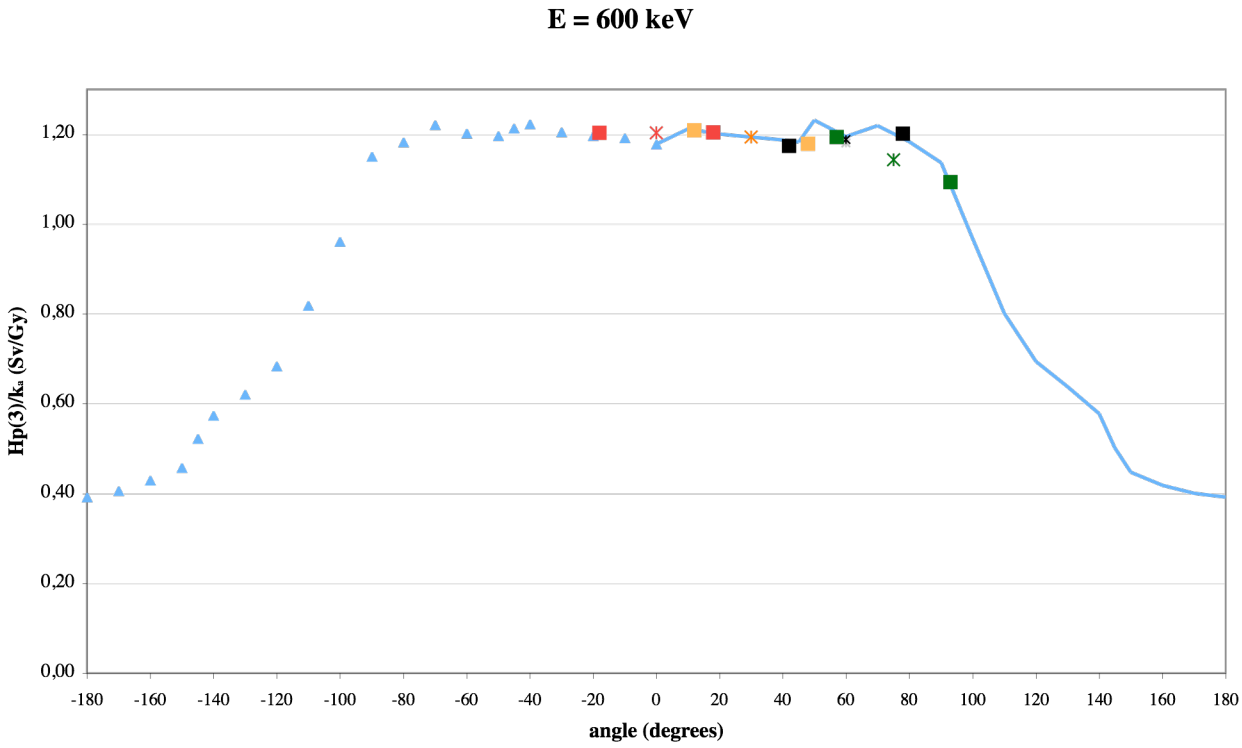

Figure A-16: $H_p(3)/k_a$ for 600 keV normally incident beam. X axis: angular scoring regions on the cylindrical phantom.

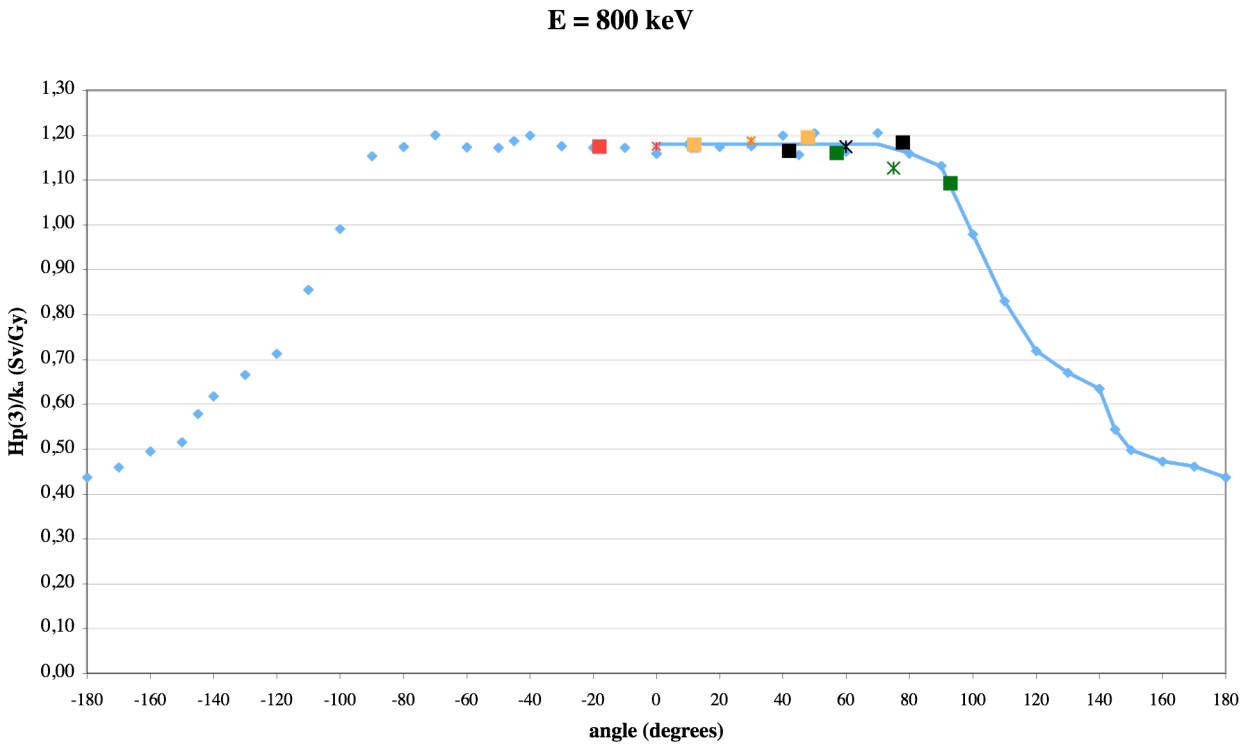

Figure A-17: $H_p(3)/k_a$ for 800 keV normally incident beam. X axis: angular scoring regions on the cylindrical phantom.

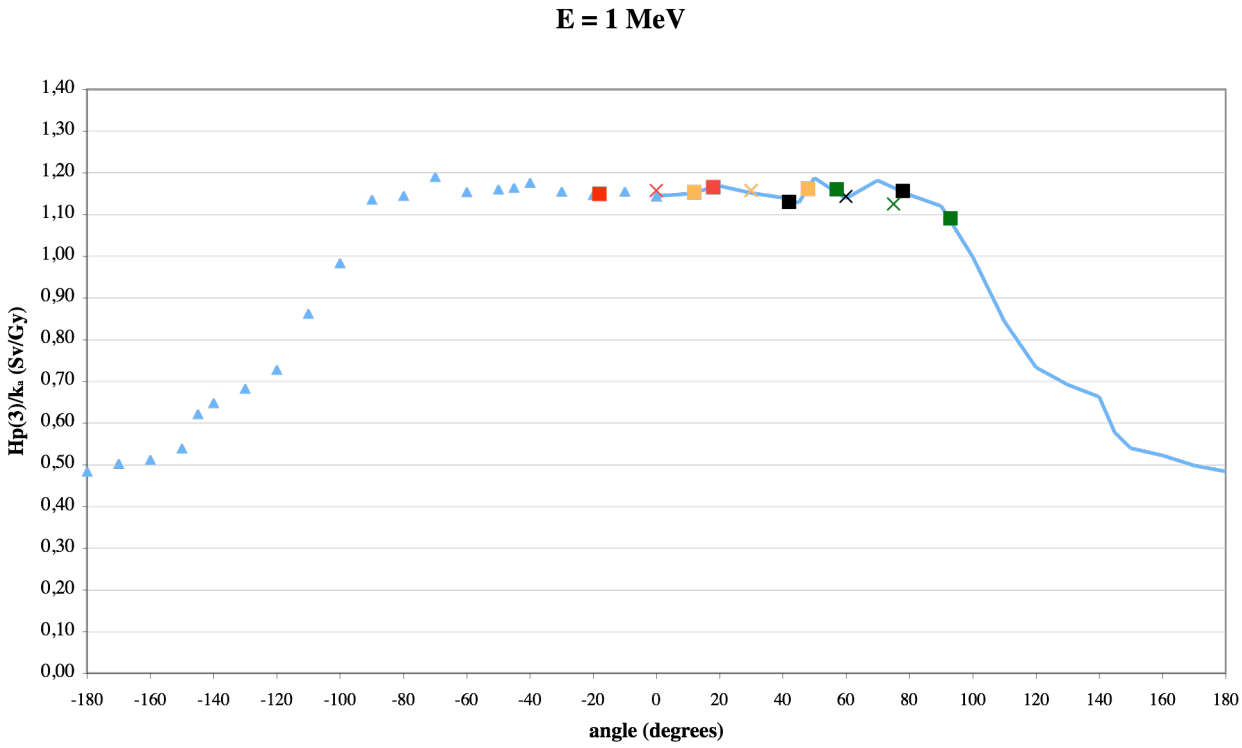

Figure A-18: $H_p(3)/k_a$ for 1 MeV normally incident beam. X axis: angular scoring regions on the cylindrical phantom.

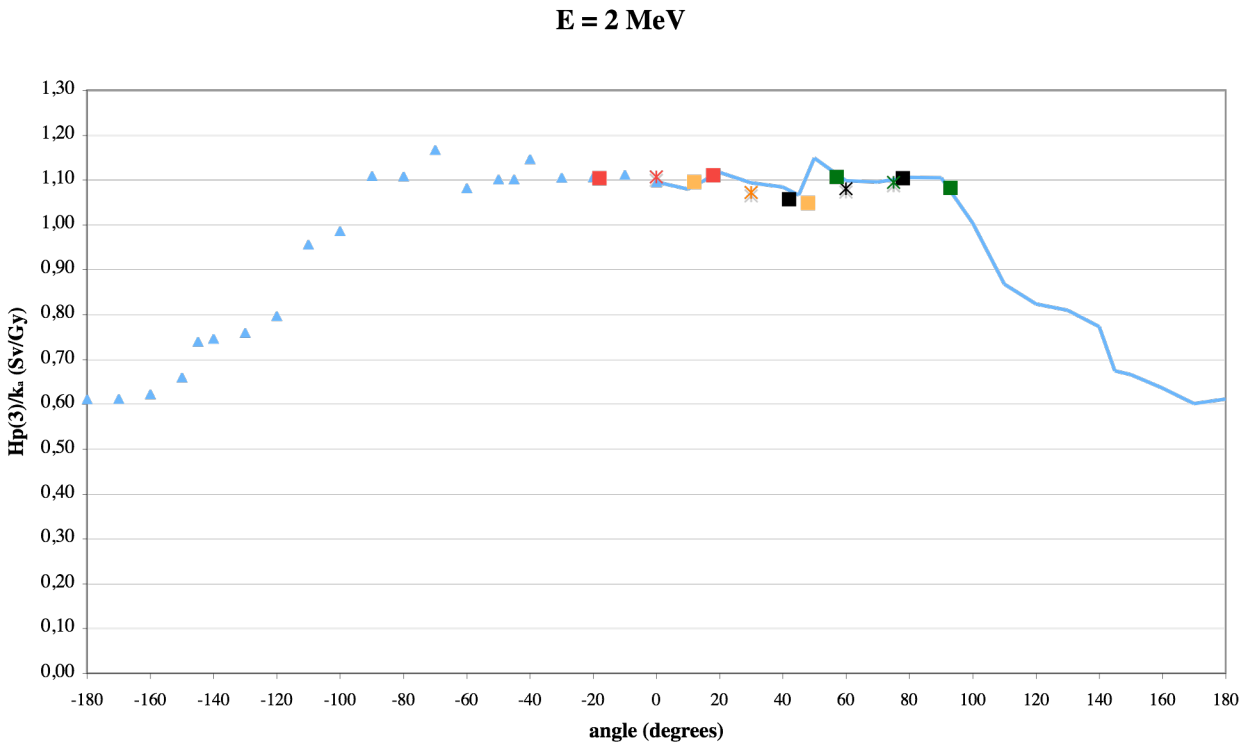

Figure A-19: $H_p(3)/k_a$ for 2 MeV normally incident beam. X axis: angular scoring regions on the cylindrical phantom.

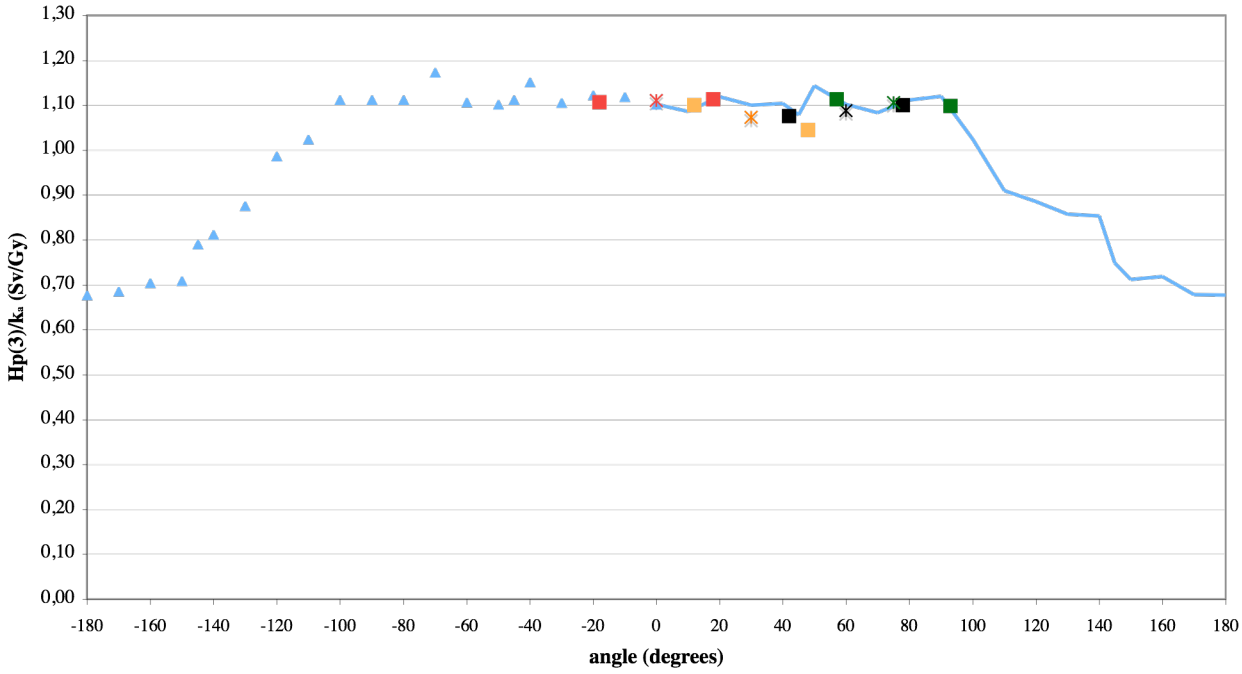

Figure A-20: $H_p(3)/k_a$ for 3 MeV normally incident beam. X axis: angular scoring regions on the cylindrical phantom.

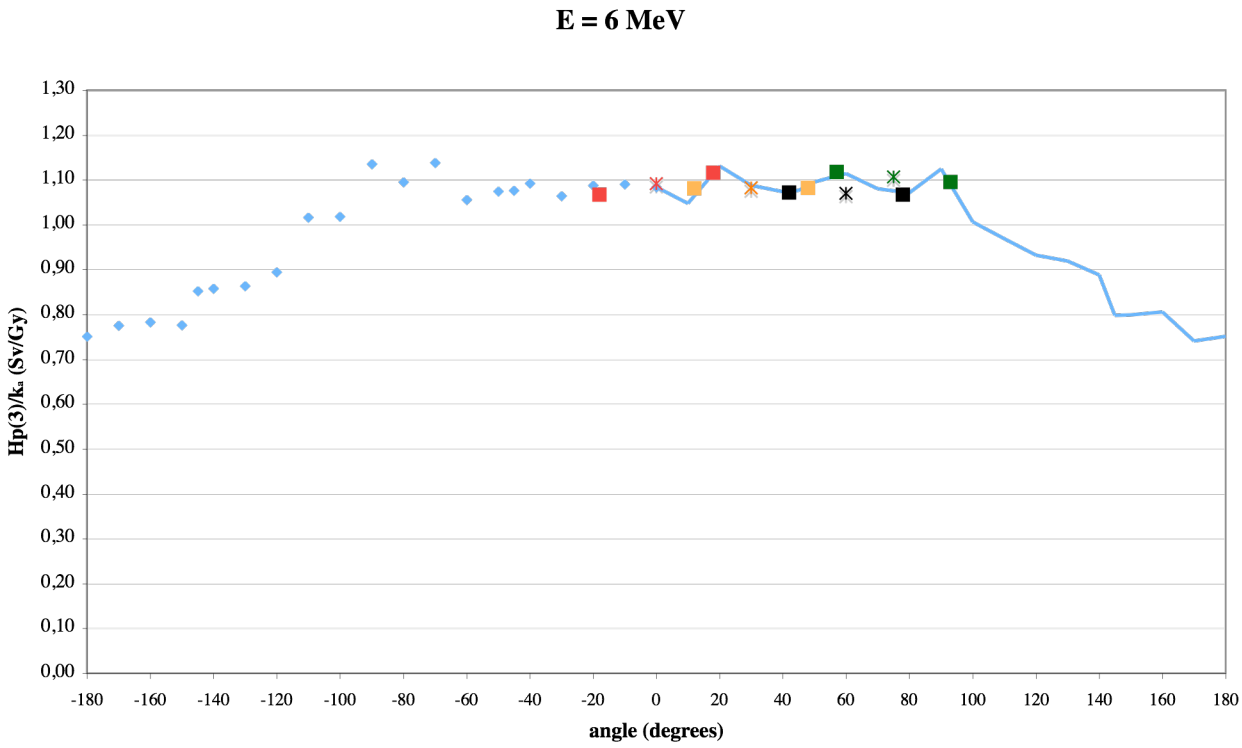

Figure A-21: $H_p(3)/k_a$ for 6 MeV normally incident beam. X axis: angular scoring regions on the cylindrical phantom.

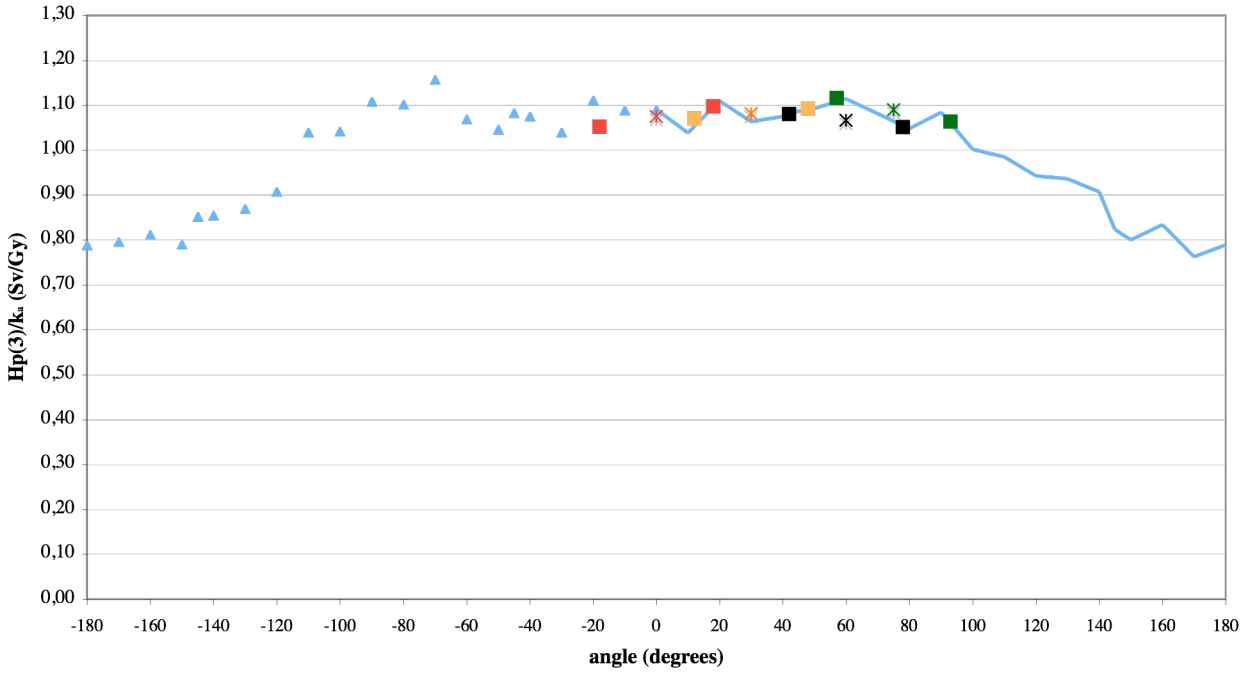

Figure A-22: $H_p(3)/k_a$ for 8 MeV normally incident beam. X axis: angular scoring regions on the cylindrical phantom.

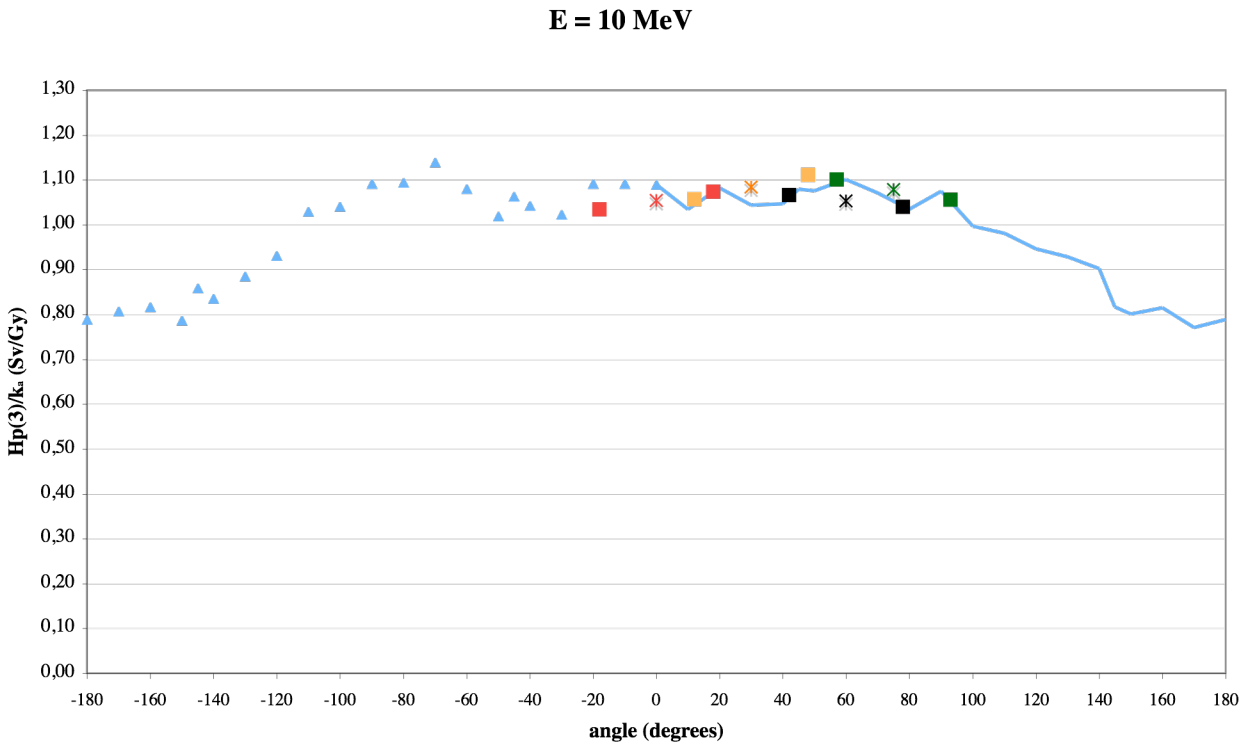

Figure A-23: $H_p(3)/k_a$ for 10 MeV normally incident beam. X axis: angular scoring regions on the cylindrical phantom.

APPENDIX B

$H_p(3)/Ka$ (E, α) (Sv/Gy) conversion coefficients as a function of energy E and angle α of incidence relative to the cylindrical phantom's main axis for expanded and aligned monoenergetic photon beams.

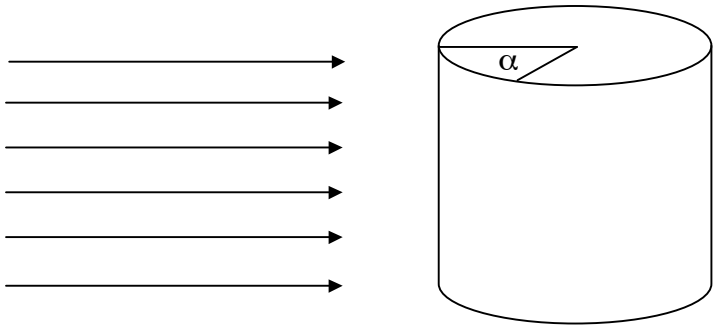

Table B-1: Angular-dependance factor R(E,α) at a depth 3 mm in the square cylindrical phantom.

		R(E, α)=(Hp(3,α)/Ka)/(Hp(3,0°)/Ka)				
E (MeV)	**Hp(3,0°)/Ka**	**10**	**15**	**20**	**30**	**40**
0,01	0,262	0,971	0,946	0,913	0,818	0,687
0,015	0,567	0,992	0,983	0,972	0,940	0,893
0,02	0,873	1,002	0,998	0,992	0,977	0,952
0,03	1,140	0,999	0,999	0,998	0,984	0,971
0,04	1,362	0,999	1,004	1,006	0,985	0,975
0,05	1,515	1,007	1,009	1,007	0,991	0,983
0,06	1,598	1,005	1,007	1,006	0,991	0,989
0,07	1,658	0,995	1,001	1,005	0,983	0,987
0,08	1,614	1,001	1,004	1,004	0,990	0,993
0,09	1,586	1,001	1,005	1,006	0,990	0,991
0,1	1,567	0,996	1,002	1,007	0,994	0,992
0,2	1,361	1,005	1,006	1,006	1,004	1,010
0,3	1,270	1,015	1,016	1,014	1,014	1,020
0,4	1,216	1,015	1,018	1,018	1,015	1,026
0,5	1,189	1,015	1,018	1,018	1,018	1,024
0,6	1,178	1,021	1,020	1,018	1,019	1,024
0,8	1,159	1,014	1,014	1,013	1,014	1,035
1	1,145	1,007	1,010	1,012	1,008	1,012
2	1,096	1,001	1,008	1,014	1,004	1,018
3	1,102	1,001	1,010	1,017	1,001	1,024
6	1,084	0,986	1,006	1,023	0,993	0,999
8	1,091	0,975	0,998	1,018	0,965	0,986
10	1,090	0,975	0,988	0,997	0,948	0,959

Table B-2 (cont.): Angular-dependance factor R(E,α) at a depth 3 mm in the square cylindrical phantom.

	R(E, α)					
E (MeV)	**45**	**50**	**60**	**70**	**75**	**80**
0,01	0,599	0,511	0,309	0,129	0,059	0,021
0,015	0,854	0,810	0,689	0,514	0,398	0,271
0,02	0,937	0,909	0,843	0,725	0,646	0,527
0,03	0,962	0,945	0,909	0,842	0,795	0,717
0,04	0,970	0,954	0,922	0,868	0,825	0,764
0,05	0,979	0,962	0,938	0,882	0,841	0,789
0,06	0,980	0,967	0,944	0,899	0,862	0,811
0,07	0,982	0,972	0,946	0,907	0,872	0,826
0,08	0,990	0,982	0,957	0,918	0,886	0,843
0,09	0,996	0,991	0,968	0,938	0,942	0,893
0,1	0,991	0,981	0,964	0,930	0,902	0,864
0,2	1,004	1,002	1,002	0,977	0,963	0,937
0,3	1,023	1,022	1,020	1,007	0,995	0,979
0,4	1,025	1,032	1,034	1,017	1,007	0,997
0,5	1,023	1,029	1,031	1,026	1,011	1,003
0,6	1,017	1,031	1,017	1,036	1,013	1,004
0,8	1,011	1,025	1,008	1,038	1,013	1,006
1	1,001	1,026	1,002	1,036	1,009	1,001
2	0,990	1,027	0,995	1,033	1,011	1,010
3	0,994	1,019	1,002	1,024	1,010	1,009
6	0,993	1,001	1,001	1,023	0,989	0,999
8	0,995	0,981	1,001	1,026	0,989	0,985
10	0,983	0,961	1,001	1,014	0,980	0,977

Table B-3 (cont.): Angular-dependance factor R(E,α) at a depth 3 mm in the square cylindrical phantom.

	R(E, α)					
E (MeV)	**90**	**100**	**110**	**120**	**130**	**135**
0,01	0,001	-	-	-	-	-
0,015	0,056	0,003	-	-	-	-
0,02	0,250	0,060	0,010	0,001	0,001	0,001
0,03	0,501	0,261	0,118	0,056	0,040	0,036
0,04	0,600	0,381	0,223	0,136	0,108	0,102
0,05	0,645	0,446	0,288	0,196	0,165	0,154
0,06	0,672	0,486	0,329	0,232	0,195	0,186
0,07	0,698	0,514	0,357	0,257	0,218	0,210
0,08	0,719	0,536	0,377	0,274	0,236	0,225
0,09	0,732	0,644	0,473	0,341	0,268	0,253
0,1	0,751	0,567	0,403	0,299	0,261	0,251
0,2	0,840	0,660	0,501	0,392	0,350	0,339
0,3	0,902	0,724	0,570	0,465	0,411	0,402
0,4	0,938	0,774	0,624	0,516	0,463	0,453
0,5	0,960	0,796	0,648	0,553	0,506	0,495
0,6	0,971	0,819	0,687	0,585	0,534	0,518
0,8	0,985	0,850	0,727	0,618	0,576	0,566
1	0,986	0,866	0,745	0,638	0,601	0,593
2	1,011	0,908	0,832	0,739	0,716	0,712
3	1,013	0,970	0,878	0,849	0,786	0,778
6	1,042	0,934	0,916	0,842	0,822	0,821
8	1,005	0,937	0,929	0,848	0,828	0,824
10	0,994	0,935	0,922	0,861	0,832	0,817

Table B-4 (cont.): Angular-dependance factor R(E,α) at a depth 3 mm in the square cylindrical phantom.

	R(E, α)					
E (MeV)	**140**	**145**	**150**	**160**	**170**	**180**
0,01	-	-	-	-	-	-
0,015	-	-	-	-	-	-
0,02	-	-	-	-	-	-
0,03	0,030	0,016	0,010	0,007	0,006	0,006
0,04	0,089	0,060	0,046	0,037	0,034	0,034
0,05	0,136	0,101	0,081	0,071	0,065	0,062
0,06	0,168	0,132	0,104	0,098	0,088	0,083
0,07	0,192	0,151	0,124	0,112	0,103	0,099
0,08	0,205	0,164	0,134	0,122	0,115	0,111
0,09	0,235	0,199	0,158	0,139	0,126	0,118
0,1	0,230	0,184	0,150	0,139	0,129	0,124
0,2	0,313	0,254	0,218	0,195	0,186	0,181
0,3	0,377	0,314	0,272	0,246	0,238	0,227
0,4	0,425	0,359	0,320	0,293	0,277	0,266
0,5	0,466	0,398	0,357	0,332	0,310	0,299
0,6	0,489	0,435	0,384	0,360	0,342	0,333
0,8	0,540	0,484	0,437	0,417	0,397	0,377
1	0,573	0,524	0,472	0,452	0,437	0,423
2	0,693	0,645	0,605	0,575	0,554	0,558
3	0,756	0,698	0,645	0,646	0,619	0,615
6	0,805	0,761	0,727	0,733	0,700	0,693
8	0,808	0,769	0,729	0,755	0,714	0,724
10	0,797	0,769	0,728	0,749	0,724	0,724

Energy dependance of the dose equivalent conversion coefficiens at depth 3 mm for selected angles of incidente for cylindrical phantom , compared with 30 cm x 30 cm x 15 cm 4-element ICRU standard tissue equivalent phantom (from GSF report) and with 15 cm x 20 cm x 20 cm 4-element ICRU standard tissue equivalent phantom (from ENEA report) .

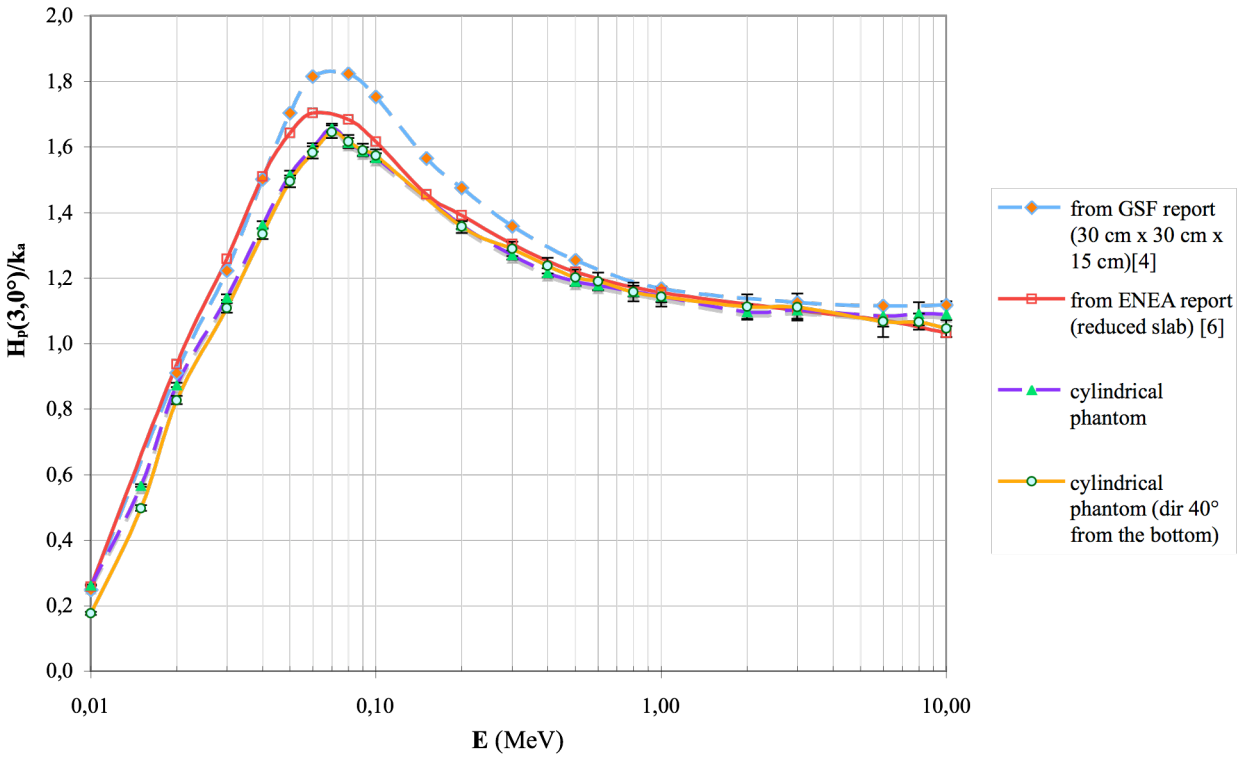

Figure B-1a

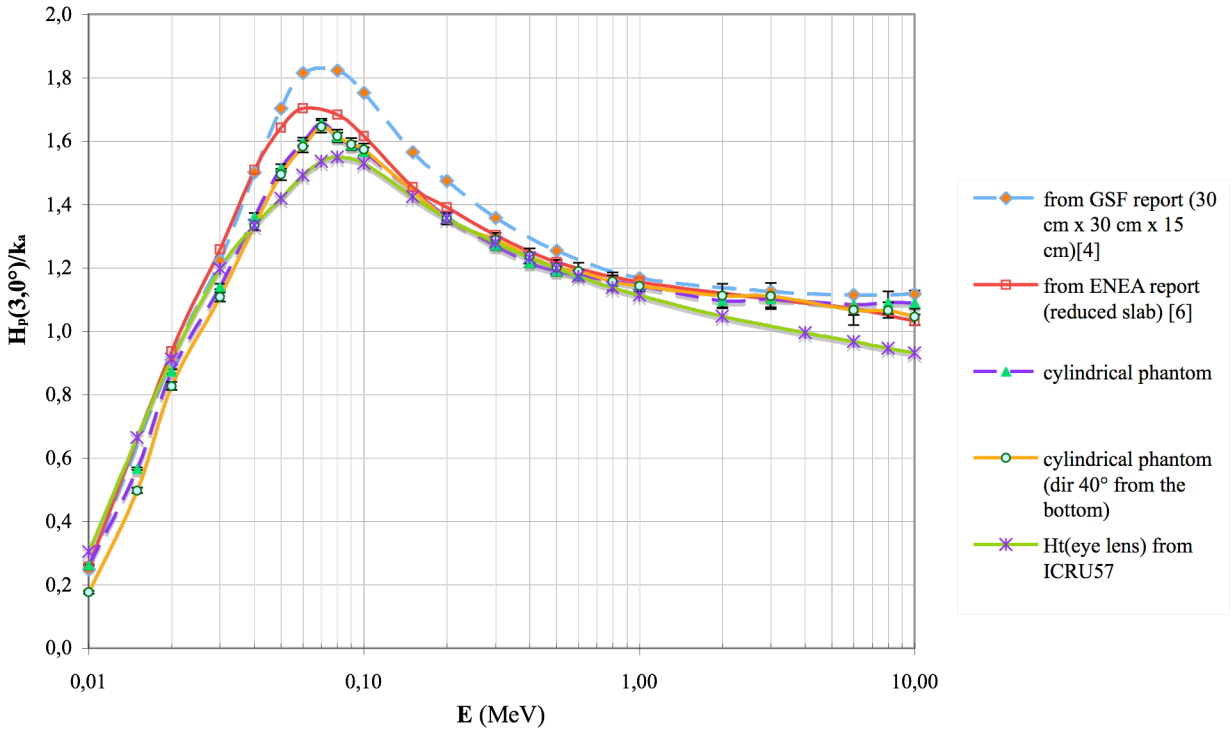

Figure B-2b (with H_T(eye lens) from ICRU57)

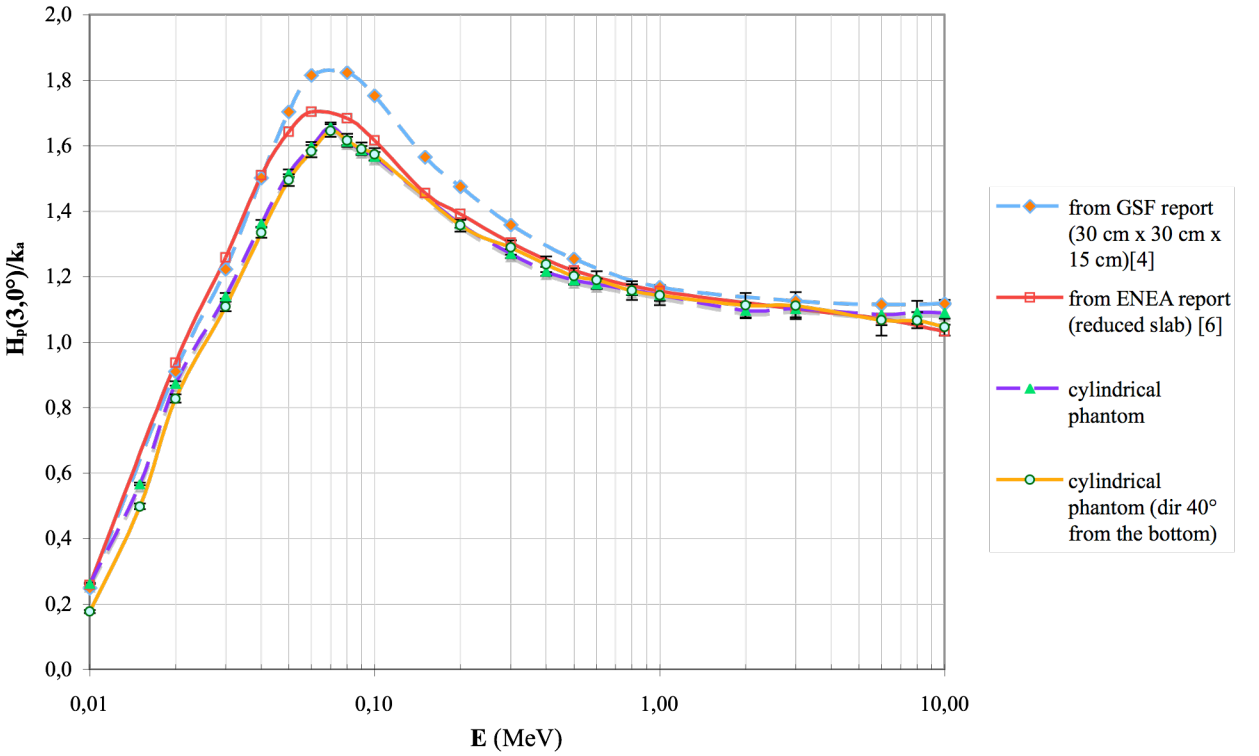

Figure B-2 (cont.)

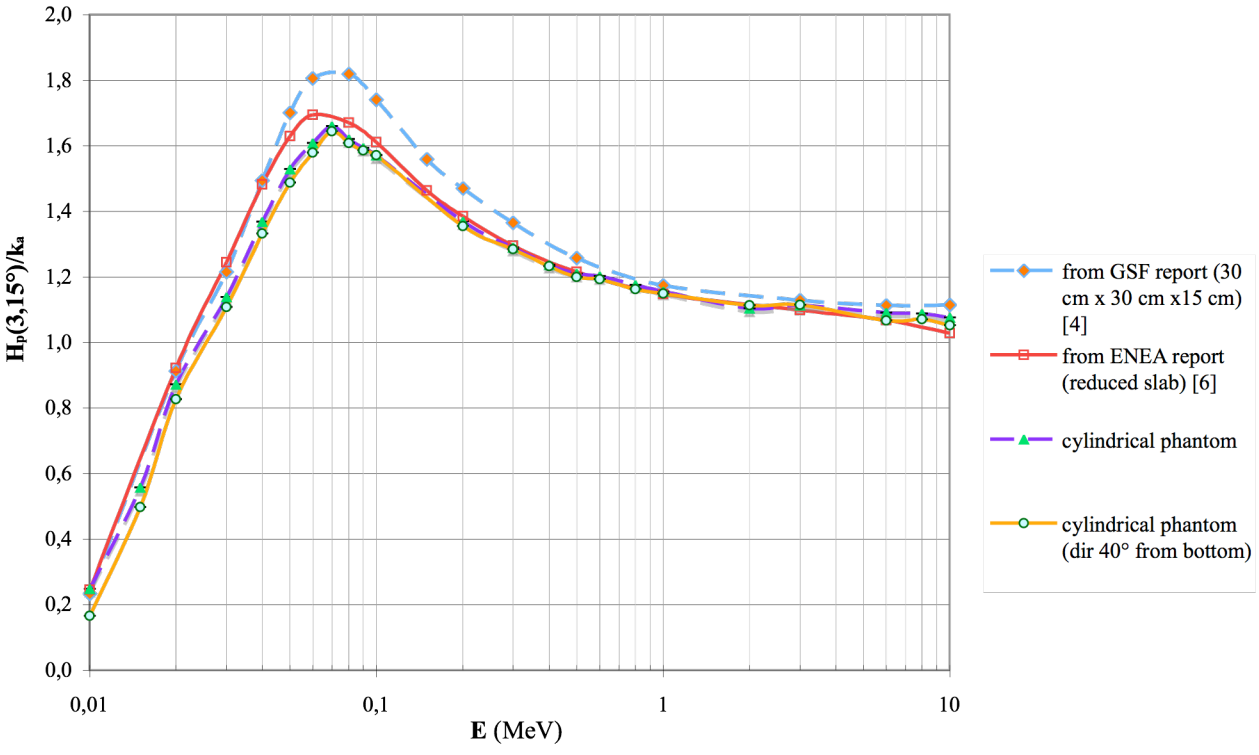

Figura B-3 (cont.)

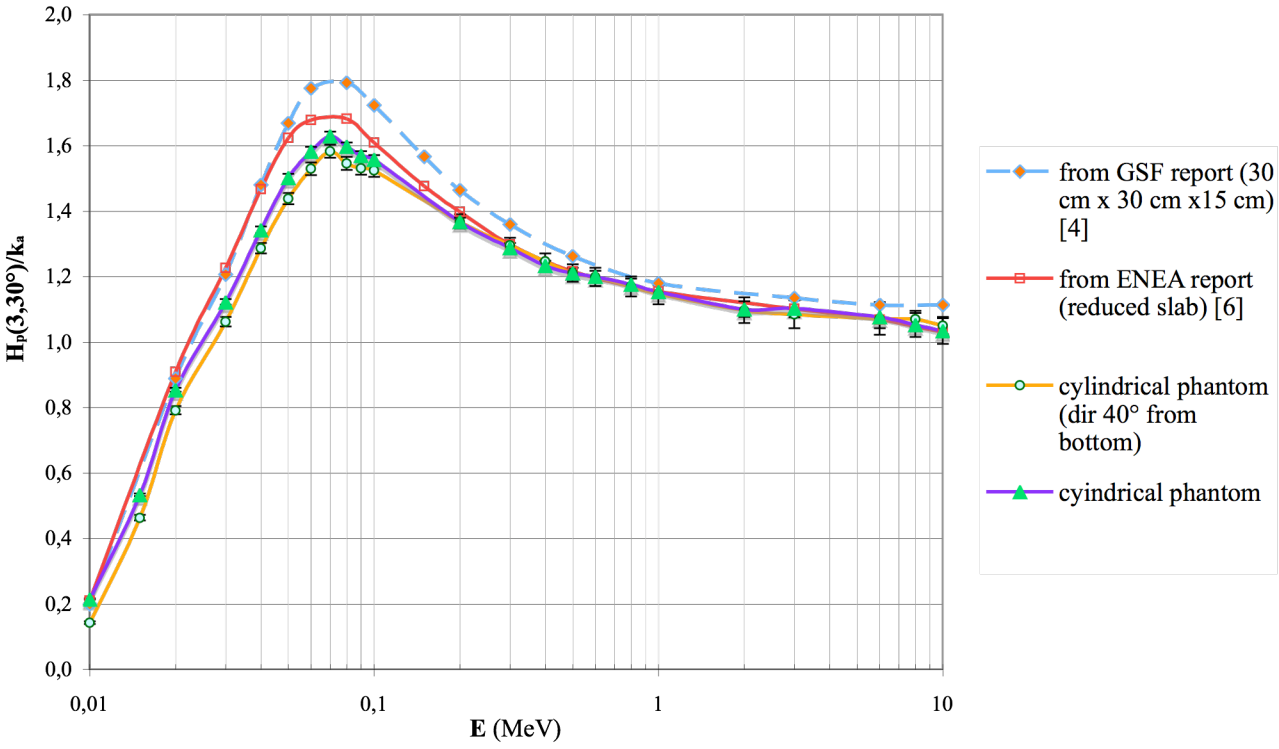

Figure B-4 (cont.)

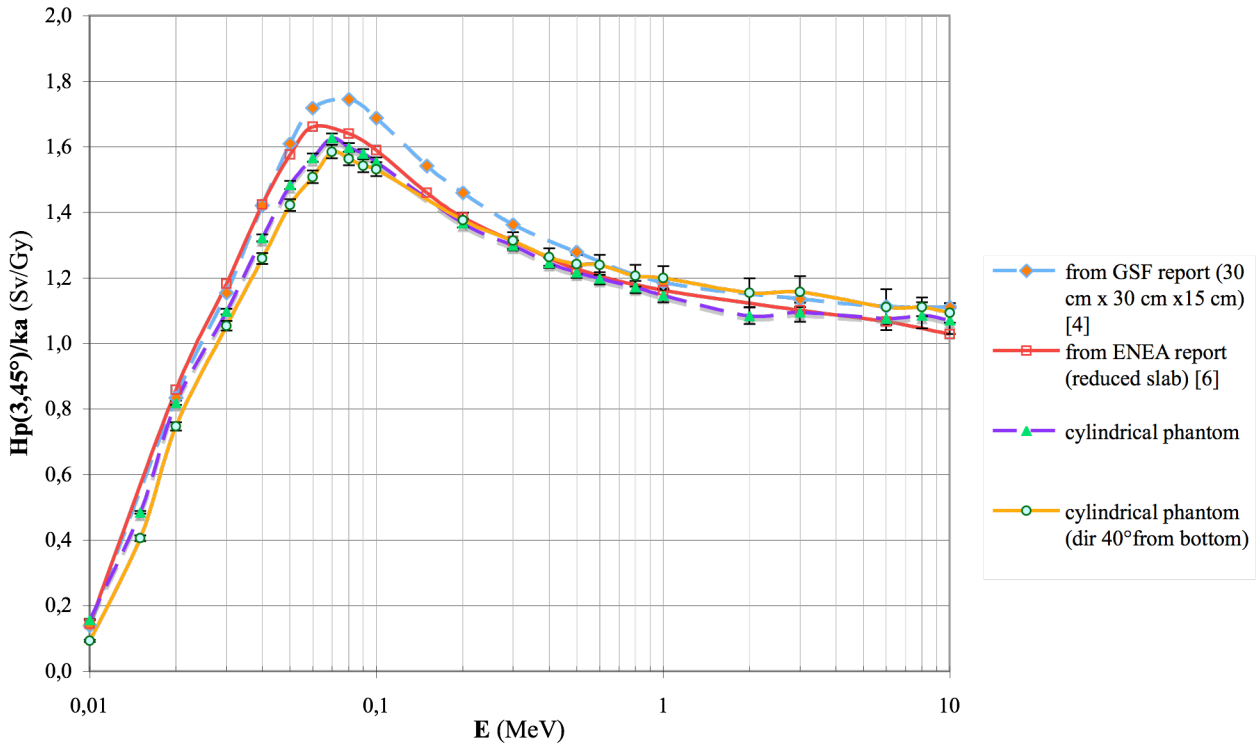

Figure B-5 (cont.)

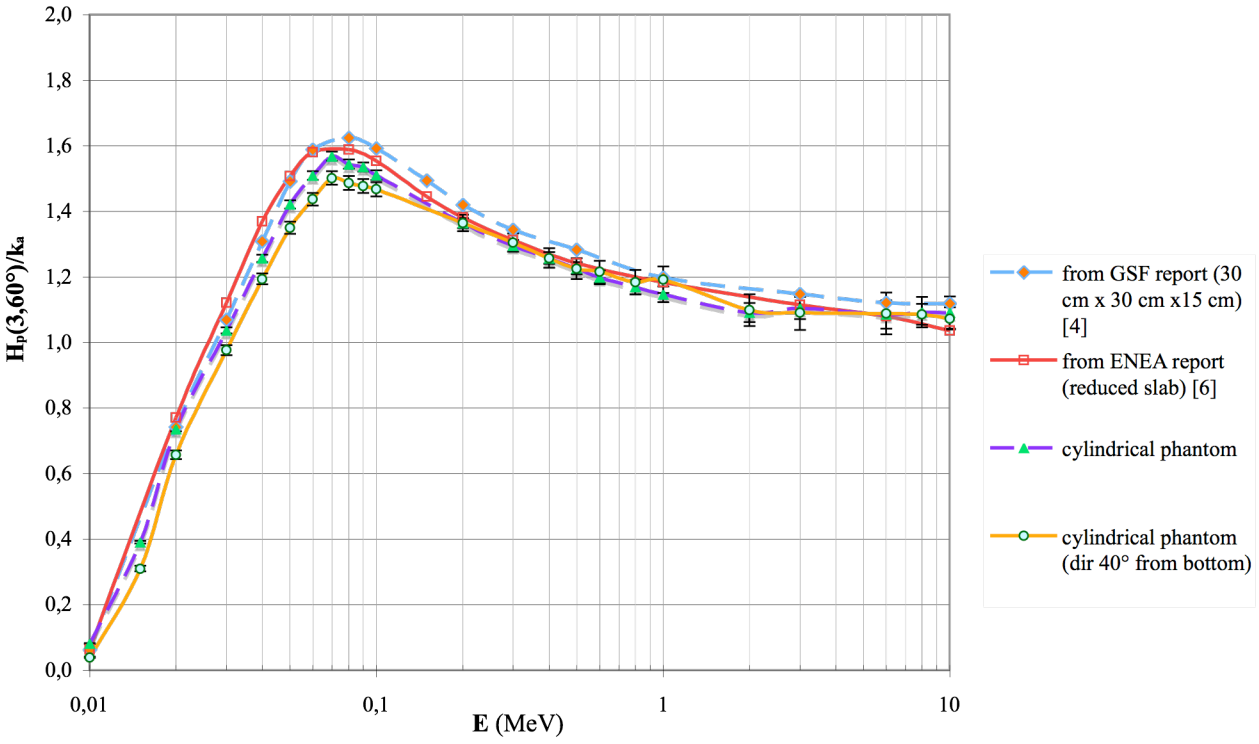

Figure B-6 (cont.)

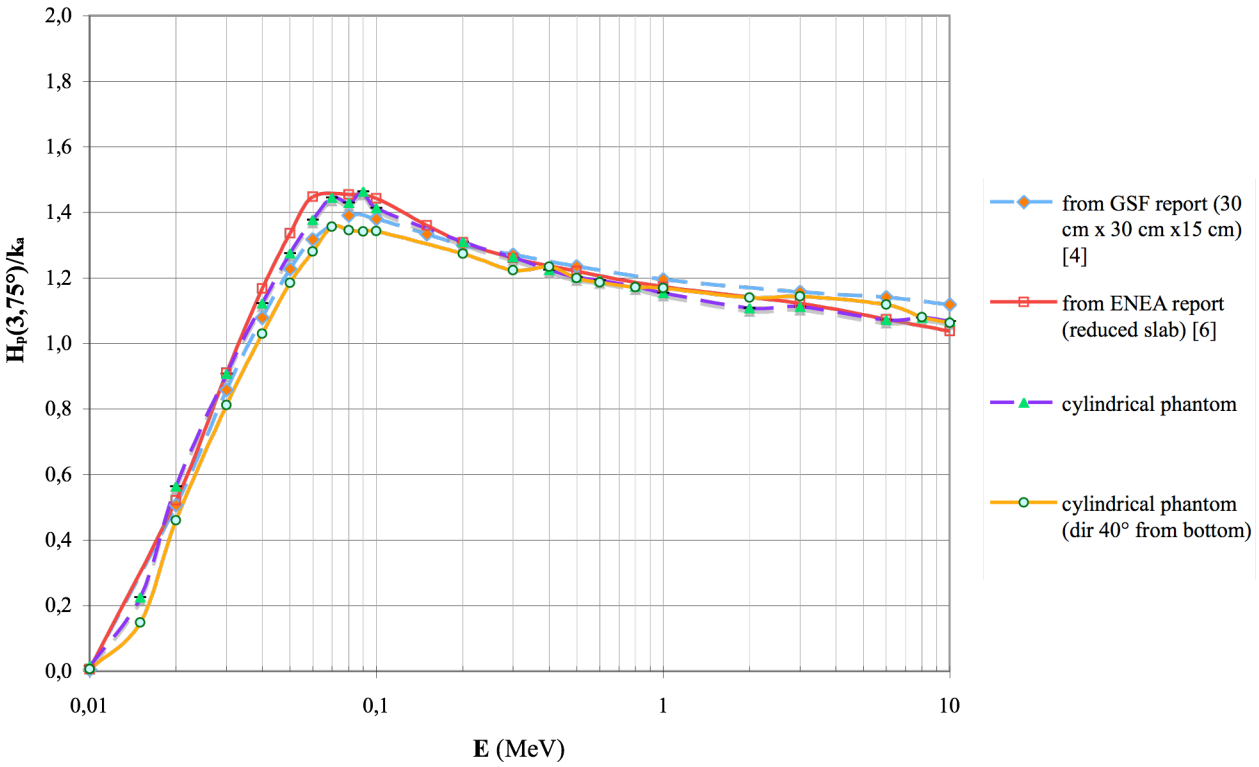

Figure B-7 (cont.)

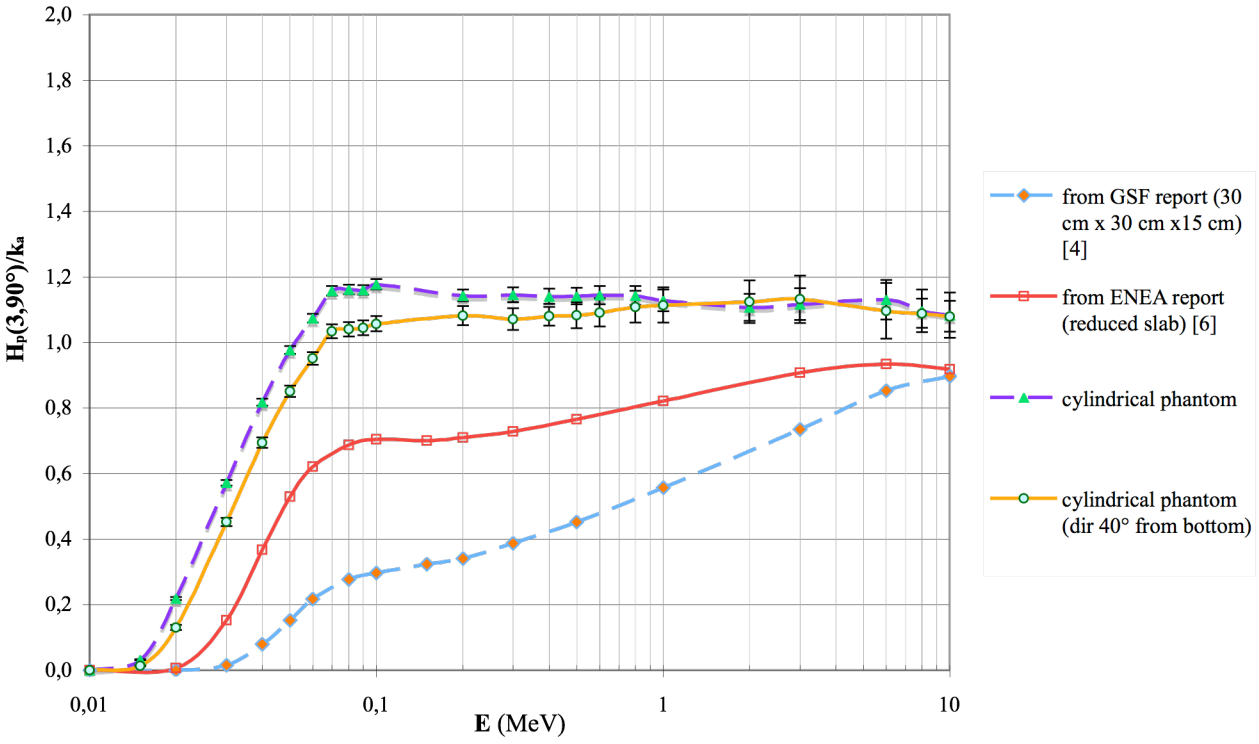

Figure B-8 (cont.)

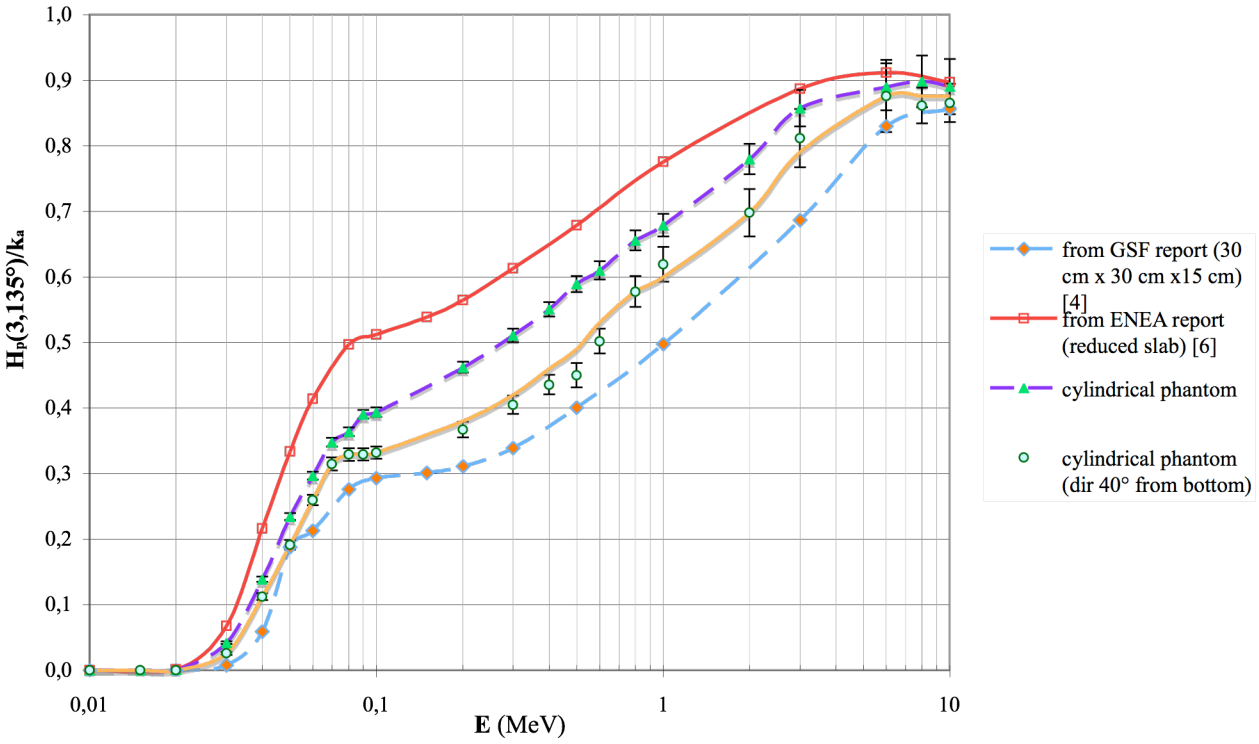

Figure B-9 (cont.)

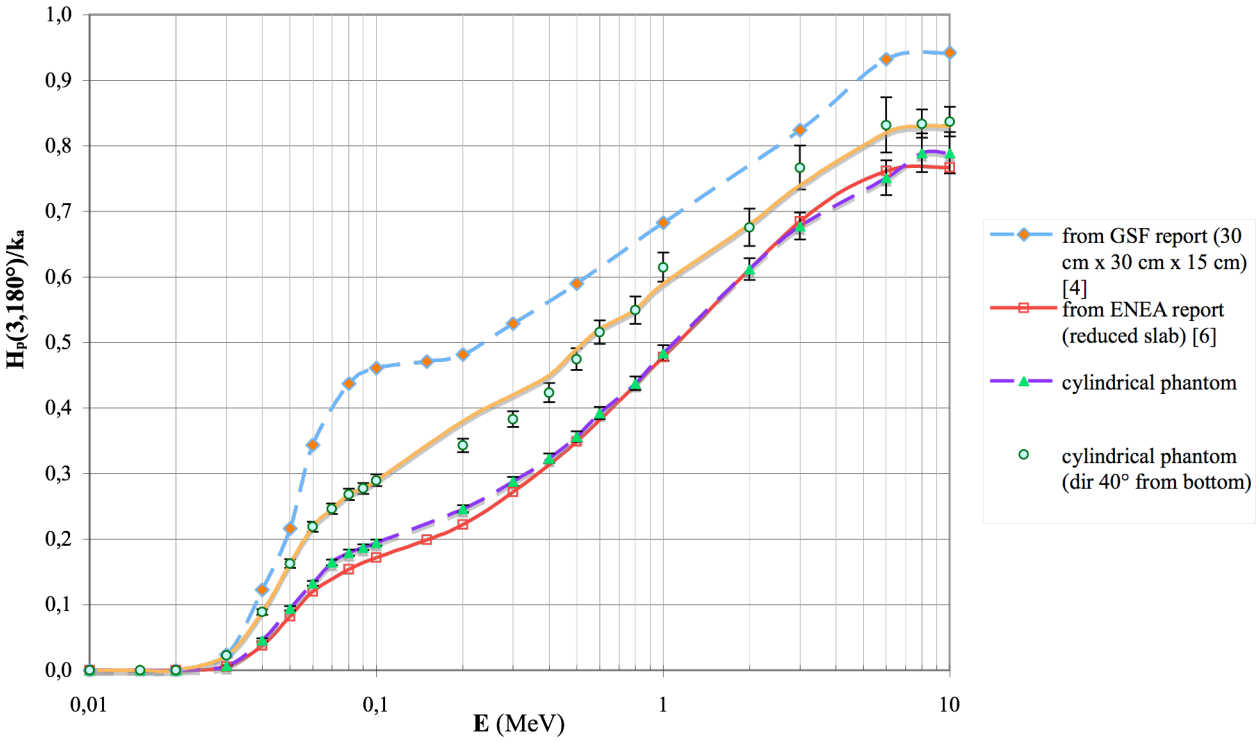

Figure B-10 (cont.)

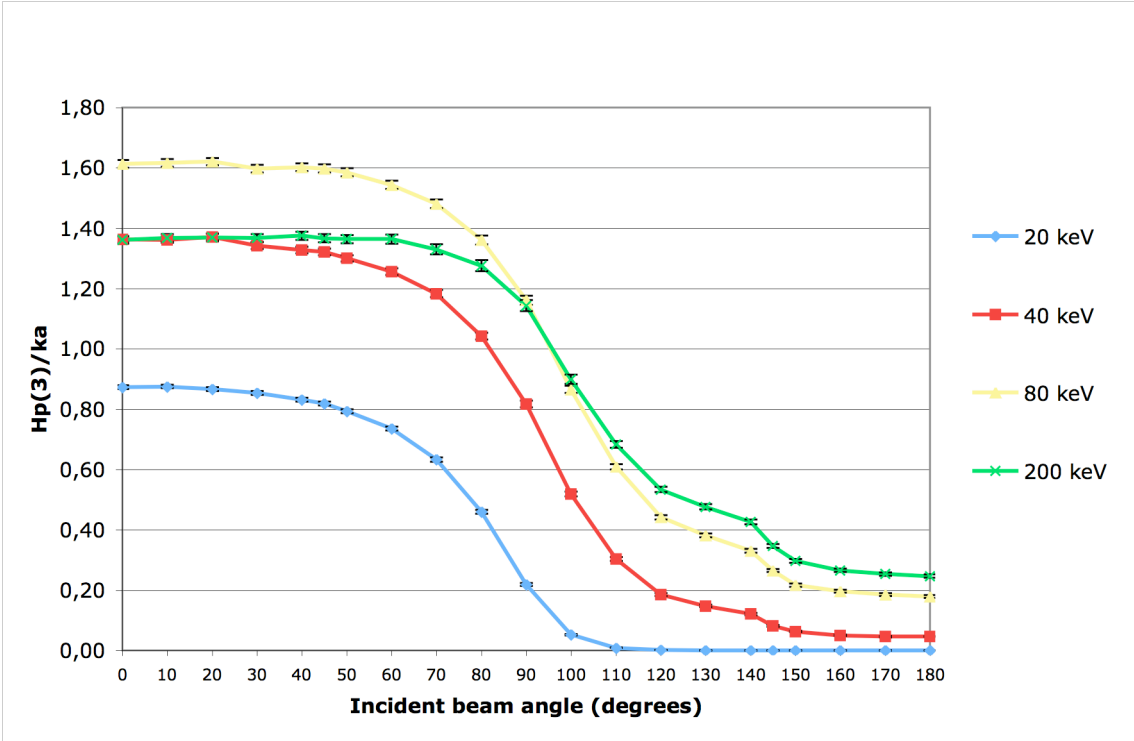

Figure B-11: $H_p(3)/Ka$ calculated for the cylindrical phatom at 20, 40, 80 and 200 keV for various incidence angles beam.

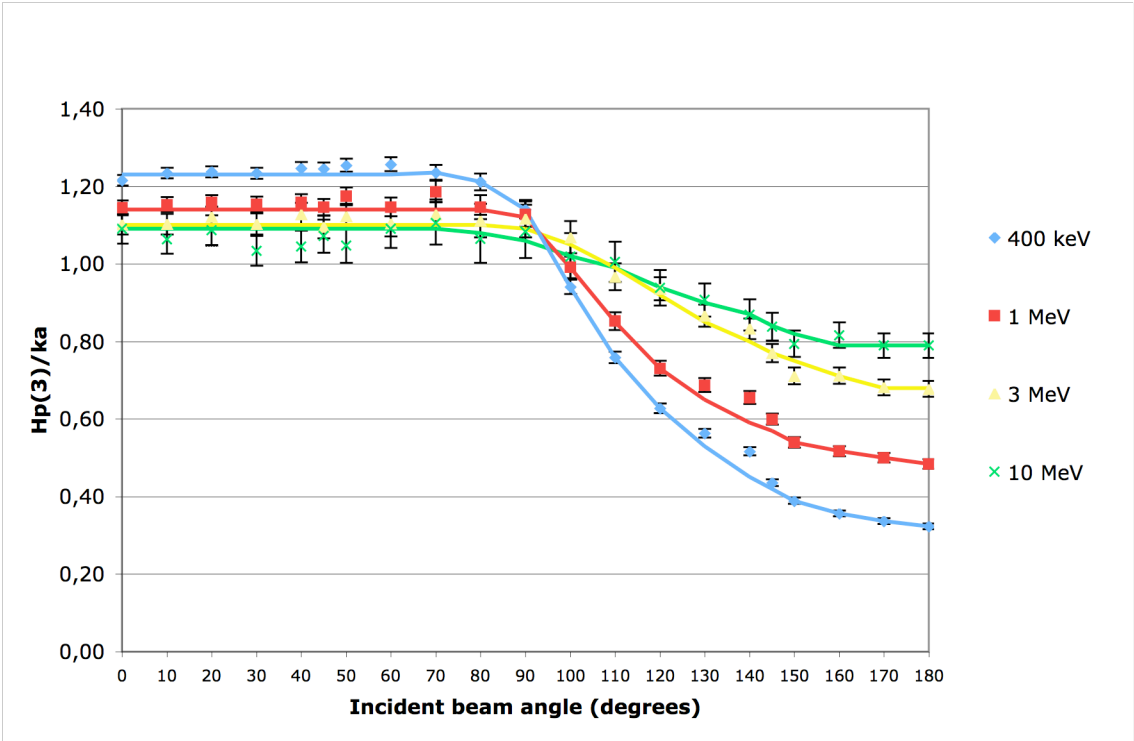

Figure B-12: $H_p(3)/Ka$ calculated for the cylindrical phatom at 400 keV, 1, 3 and 10 MeV for various incidence angles beam.

APPENDIX C

$H_p(3)/Ka$ (E, α) (Sv/Gy) conversion coefficients as a function of energy E and angle α of incidence for the 40° incident from the bottom of the radiation beam.

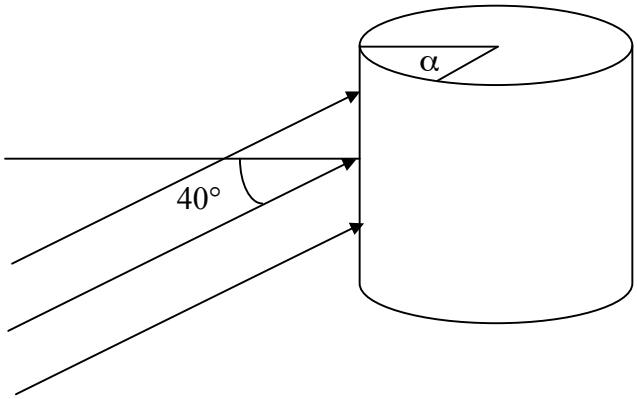

Table C-1: Angular-dependance factor R(E,α) at a depth 3 mm in the square cylindrical phantom.

		R(E, α)=(Hp(3,α)/Ka)/(Hp(3,0°)/Ka)				
E (MeV)	**Hp(3,0°)/Ka**	**10**	**15**	**20**	**30**	**40**
0,01	0,176	0,970	0,941	0,901	0,790	0,630
0,015	0,498	0,993	0,979	0,962	0,932	0,886
0,02	0,827	0,995	0,983	0,971	0,962	0,930
0,03	1,108	0,994	0,989	0,983	0,968	0,954
0,04	1,334	0,990	0,985	0,980	0,975	0,961
0,05	1,495	0,982	0,981	0,981	0,972	0,955
0,06	1,583	0,988	0,983	0,979	0,970	0,959
0,07	1,646	0,992	0,986	0,979	0,970	0,964
0,08	1,616	0,980	0,977	0,975	0,967	0,963
0,09	1,590	0,986	0,981	0,977	0,976	0,966
0,1	1,573	0,988	0,982	0,976	0,977	0,970
0,2	1,357	0,998	1,001	1,005	1,015	1,010
0,3	1,288	0,992	0,995	1,001	1,011	1,007
0,4	1,237	0,982	0,983	0,988	1,008	1,011
0,5	1,201	0,996	0,997	0,999	1,015	1,023
0,6	1,190	1,000	0,992	0,987	1,015	1,019
0,8	1,157	1,006	0,997	0,989	1,017	1,023
1	1,143	1,006	0,990	0,977	1,009	1,025
2	1,113	0,986	0,973	0,964	0,988	1,018
3	1,111	0,998	0,982	0,968	0,981	1,014
6	1,067	1,002	1,006	1,006	0,988	1,015
8	1,066	1,008	0,997	0,988	1,012	1,015
10	1,045	1,018	1,004	0,992	1,018	1,017

Table C-2 (cont.)

	R(E, α)					
E (MeV)	**45**	**50**	**60**	**70**	**75**	**80**
0,01	0,527	0,429	0,222	0,072	0,036	0,014
0,015	0,816	0,769	0,622	0,417	0,298	0,188
0,02	0,903	0,872	0,794	0,642	0,556	0,430
0,03	0,951	0,922	0,881	0,786	0,733	0,644
0,04	0,944	0,922	0,895	0,817	0,772	0,705
0,05	0,951	0,934	0,903	0,834	0,793	0,734
0,06	0,953	0,941	0,908	0,845	0,809	0,756
0,07	0,963	0,947	0,912	0,855	0,825	0,776
0,08	0,967	0,943	0,920	0,865	0,832	0,785
0,09	0,970	0,951	0,929	0,875	0,844	0,797
0,1	0,974	0,955	0,933	0,884	0,854	0,810
0,2	1,015	1,002	1,005	0,959	0,939	0,910
0,3	1,019	0,999	1,013	0,963	0,950	0,928
0,4	1,021	1,007	1,016	0,978	0,957	0,950
0,5	1,034	1,017	1,020	0,999	0,999	0,986
0,6	1,042	1,027	1,021	1,009	0,997	0,985
0,8	1,043	1,040	1,023	1,011	1,012	1,011
1	1,050	1,037	1,042	1,014	1,024	1,026
2	1,038	1,033	0,987	1,008	1,025	1,039
3	1,042	1,044	0,983	1,015	1,029	1,041
6	1,041	1,067	1,020	1,050	1,048	1,050
8	1,042	1,024	1,018	1,010	1,014	1,024
10	1,046	1,027	1,026	1,025	1,017	1,025

Table C-3 (cont.)

	R(E, α)					
E (MeV)	**90**	**100**	**110**	**120**	**130**	**135**
0,01	-	-	-	-	-	-
0,015	0,028	0,001	-	-	-	-
0,02	0,157	0,025	0,003	0,001	0,000	0,000
0,03	0,408	0,172	0,068	0,032	0,027	0,023
0,04	0,520	0,288	0,154	0,095	0,084	0,084
0,05	0,569	0,355	0,214	0,144	0,132	0,128
0,06	0,601	0,387	0,253	0,181	0,161	0,164
0,07	0,628	0,418	0,276	0,198	0,175	0,191
0,08	0,643	0,433	0,296	0,208	0,194	0,203
0,09	0,657	0,448	0,309	0,218	0,202	0,207
0,1	0,672	0,461	0,315	0,225	0,209	0,211
0,2	0,797	0,562	0,405	0,301	0,275	0,271
0,3	0,831	0,619	0,451	0,354	0,331	0,314
0,4	0,921	0,778	0,442	0,390	0,353	0,352
0,5	0,902	0,707	0,541	0,432	0,409	0,375
0,6	0,918	0,722	0,557	0,462	0,436	0,422
0,8	0,958	0,764	0,613	0,519	0,501	0,499
1	0,975	0,793	0,644	0,552	0,524	0,542
2	1,010	0,833	0,748	0,654	0,616	0,627
3	1,019	0,870	0,816	0,718	0,693	0,730
6	1,027	0,901	0,888	0,823	0,806	0,821
8	1,021	0,908	0,879	0,816	0,812	0,808
10	1,033	0,926	0,894	0,824	0,829	0,828

Table C-4 (cont.)

	R(E, α)					
E (MeV)	**140**	**145**	**150**	**160**	**170**	**180**
0,01	-	-	-	-	-	-
0,015	-	-	-	-	-	-
0,02	-	-	-	-	0,001	-
0,03	0,022	0,022	0,020	0,019	0,022	0,020
0,04	0,079	0,072	0,068	0,069	0,069	0,067
0,05	0,123	0,117	0,111	0,110	0,107	0,109
0,06	0,156	0,145	0,138	0,138	0,140	0,138
0,07	0,179	0,161	0,159	0,155	0,157	0,150
0,08	0,189	0,172	0,174	0,168	0,171	0,166
0,09	0,196	0,183	0,180	0,177	0,182	0,174
0,1	0,202	0,190	0,184	0,188	0,192	0,184
0,2	0,262	0,256	0,257	0,259	0,257	0,253
0,3	0,303	0,301	0,310	0,311	0,308	0,297
0,4	0,348	0,347	0,357	0,355	0,362	0,342
0,5	0,372	0,385	0,398	0,401	0,394	0,395
0,6	0,412	0,413	0,431	0,429	0,434	0,434
0,8	0,471	0,453	0,484	0,486	0,493	0,475
1	0,509	0,486	0,533	0,524	0,525	0,538
2	0,598	0,579	0,618	0,594	0,627	0,607
3	0,690	0,651	0,692	0,664	0,686	0,690
6	0,763	0,716	0,762	0,760	0,779	0,779
8	0,784	0,770	0,794	0,791	0,792	0,782
10	0,804	0,788	0,811	0,811	0,806	0,800

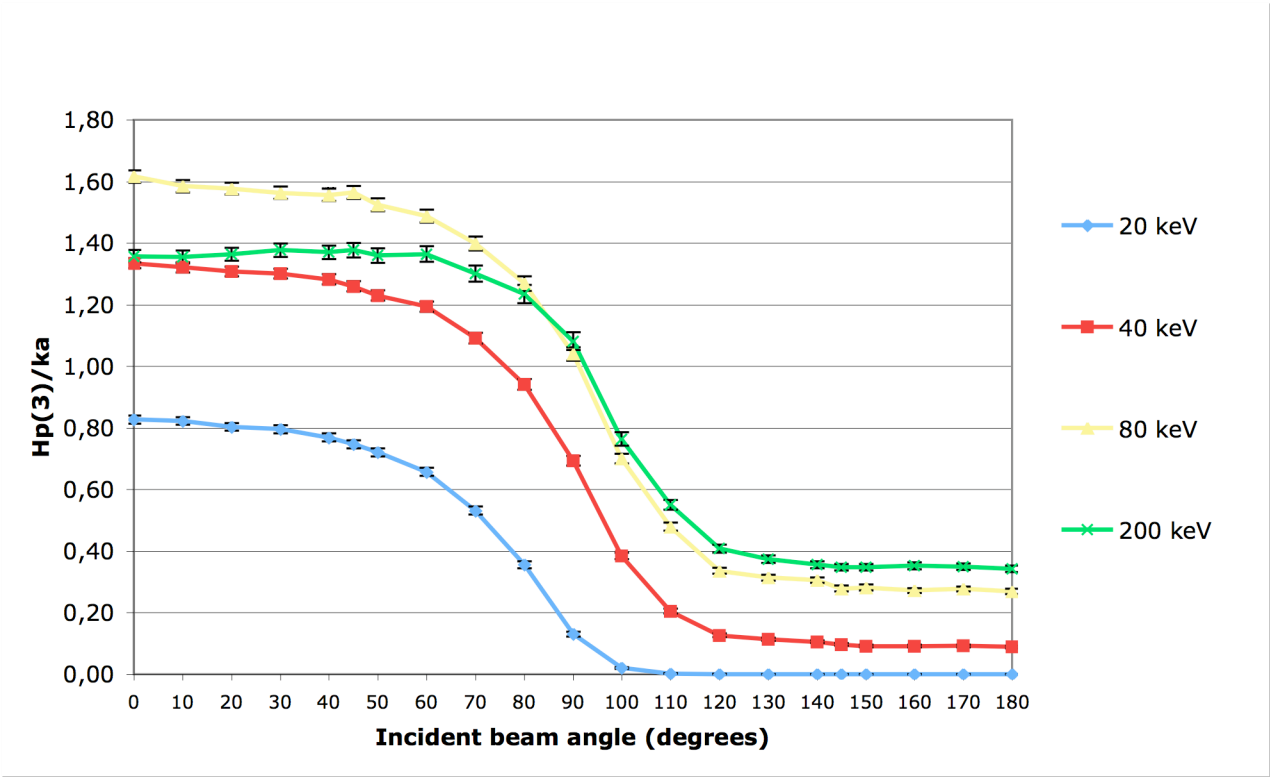

Figure C-1: $H_p(3)/k_a$ calculated for the cylindrical phatom at 20, 40, 80 and 200 keV for various incidence angles beam with the beam incident with an angle of 40° on the cylinder axis main.

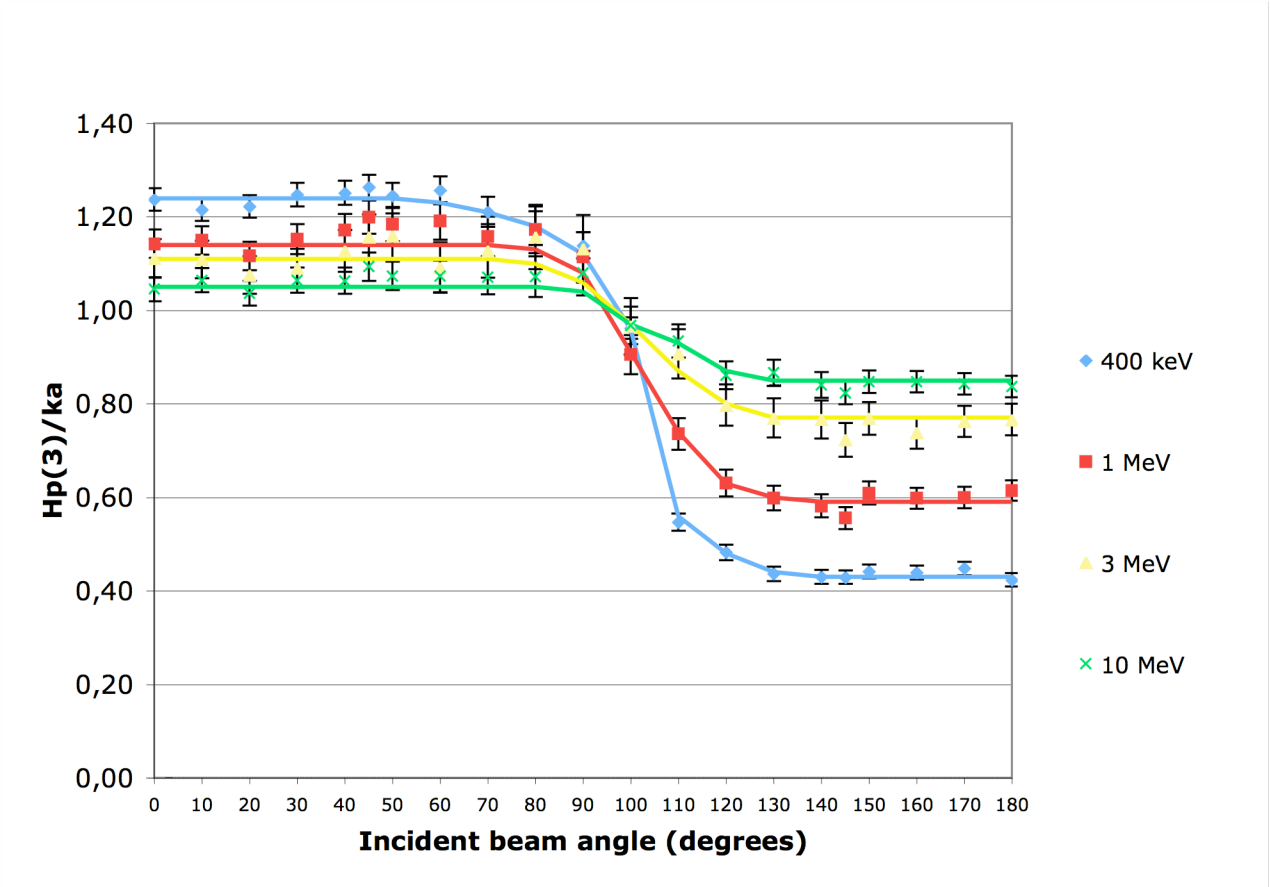

Figure C-2: $Hp(3)/k_a$ calculated for the cylindrical phatom at 400 keV, 1, 3 and 10 M eV for various incidence angles beam with the beam incident with an angle of 40° on the cylinder axis main.

APPENDIX D

Air kerma backscatter factor (B) for the cylindrical 20 cm x 20 cm phantom at various distances from phantom surface for a normally incident beam.

(ISO slab standard and reduced phantom values are reported for comparison only for normal incidence)

E (keV) is the mean energy of the spectrum.

*** distance from the phantom, d = 0 mm**

	E (keV)								
angles (°)	**33**	**47**	**65**	**83**	**100**	**117**	**163**	**207**	**248**
0	1,359	1,554	1,567	1,497	1,429	1,369	1,271	1,218	1,184
20	1,359	1,547	1,561	1,494	1,425	1,364	1,271	1,219	1,186
40	1,346	1,527	1,545	1,481	1,419	1,366	1,279	1,230	1,197
60	1,312	1,484	1,509	1,462	1,409	1,362	1,286	1,243	1,212
75	1,277	1,434	1,467	1,433	1,393	1,354	1,292	1,254	1,231

*** distance from the phantom, d = 1 mm**

	E (keV)								
angles (°)	**33**	**47**	**65**	**83**	**100**	**117**	**163**	**207**	**248**
0	1,337	1,524	1,537	1,471	1,406	1,348	1,255	1,206	1,173
20	1,337	1,517	1,529	1,465	1,402	1,344	1,255	1,206	1,174
40	1,320	1,494	1,510	1,452	1,392	1,343	1,260	1,213	1,183
60	1,286	1,451	1,476	1,433	1,382	1,336	1,267	1,226	1,197
75	1,241	1,394	1,428	1,398	1,360	1,323	1,265	1,231	1,208

*** distance from the phantom, d = 5 mm**

	E (keV)								
angles (°)	**33**	**47**	**65**	**83**	**100**	**117**	**163**	**207**	**248**
0	1,292	1,453	1,461	1,406	1,347	1,298	1,219	1,174	1,146
20	1,287	1,443	1,452	1,398	1,343	1,293	1,217	1,174	1,146
40	1,270	1,414	1,433	1,382	1,332	1,287	1,216	1,178	1,152
60	1,234	1,373	1,394	1,357	1,315	1,277	1,217	1,182	1,160
75	1,194	1,324	1,354	1,329	1,297	1,266	1,217	1,189	1,171

*** distance from the phantom, d = 10,5 mm**

	E (keV)								
angles (°)	**33**	**47**	**65**	**83**	**100**	**117**	**163**	**207**	**248**
0	1,263	1,407	1,413	1,361	1,310	1,264	1,193	1,154	1,129
20	1,257	1,397	1,403	1,355	1,305	1,263	1,193	1,155	1,130
40	1,237	1,366	1,379	1,337	1,292	1,251	1,189	1,154	1,132
60	1,203	1,324	1,341	1,307	1,271	1,238	1,185	1,156	1,136
75	1,165	1,280	1,308	1,285	1,257	1,231	1,188	1,163	1,146

*** distance from the phantom, d = 20,5 mm**

	E (keV)								
angles (°)	**33**	**47**	**65**	**83**	**100**	**117**	**163**	**207**	**248**
0	1,219	1,338	1,340	1,296	1,254	1,217	1,156	1,125	1,105
20	1,214	1,327	1,333	1,291	1,249	1,214	1,156	1,125	1,105
40	1,193	1,299	1,307	1,273	1,236	1,202	1,152	1,124	1,105
60	1,159	1,254	1,271	1,245	1,216	1,190	1,147	1,122	1,106
75	1,131	1,220	1,244	1,226	1,203	1,182	1,147	1,127	1,113

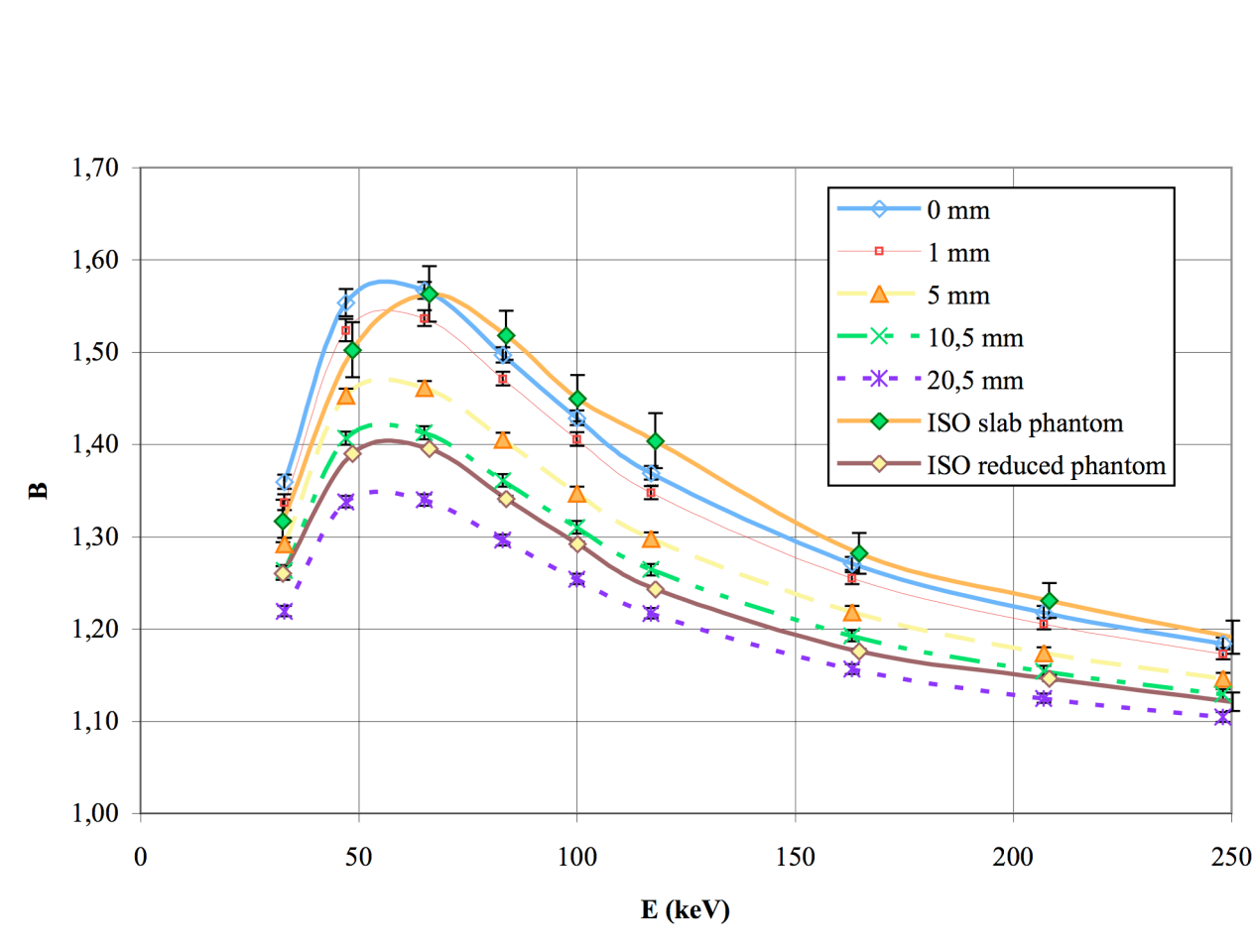

Figure D-1: Air kerma backscatter factors of the employed phantom for normal incident beam and ISO narrow beam series of the beams mean energy at various distance from phantom surface.

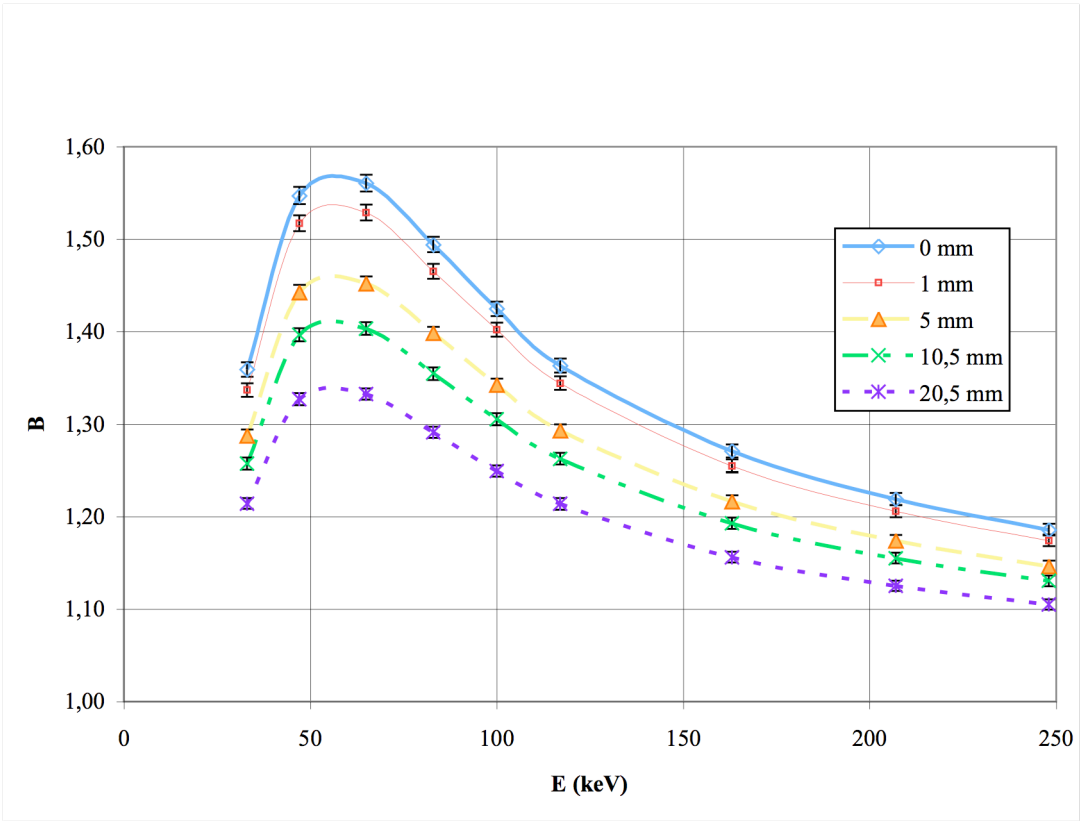

Figure D-2: Air kerma backscatter factors of the employed phantom for 20° incident beam at various distance from phantom surface.

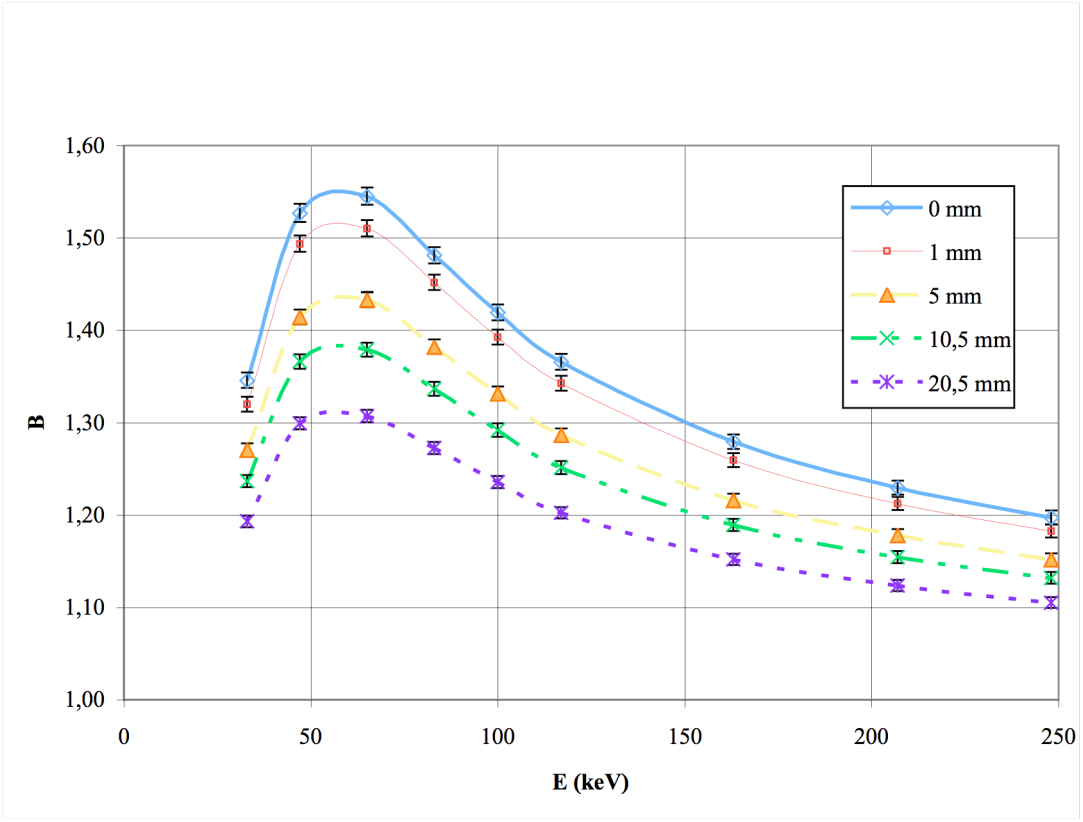

Figure D-3: Air kerma backscatter factors of the employed phantom for 40° incident beam at various distance from phantom surface.

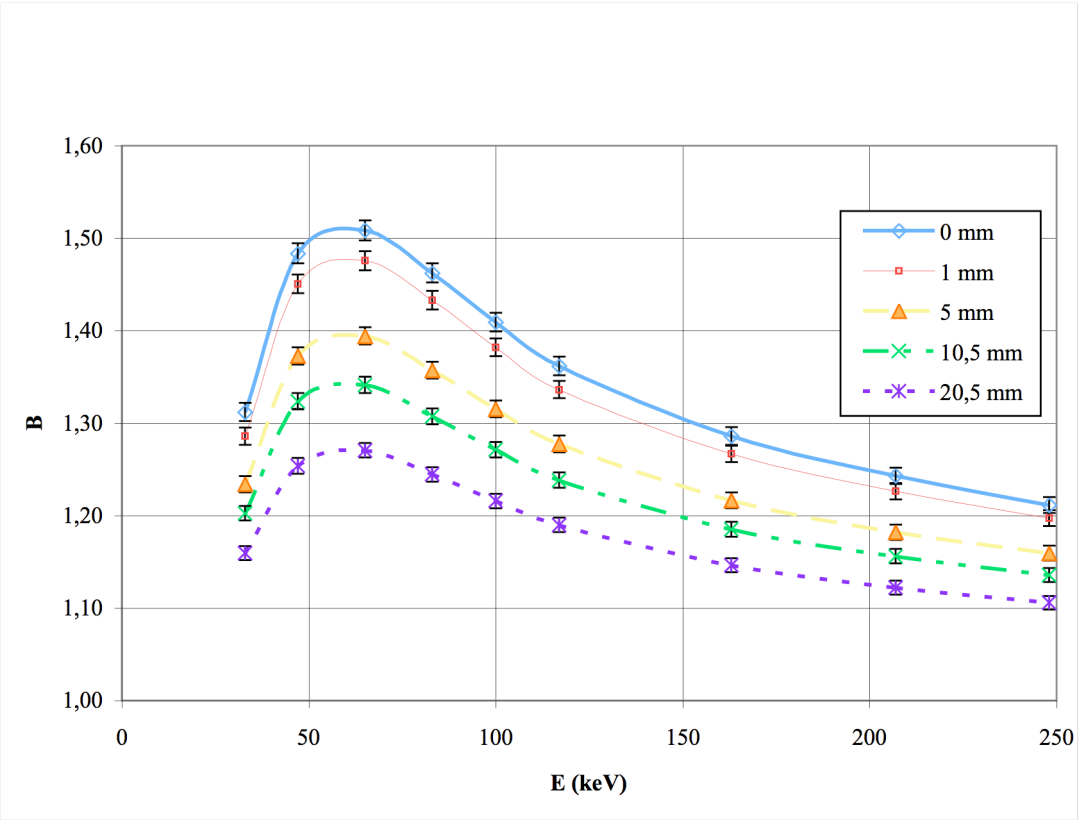

Figure D-4: Air kerma backscatter factors of the employed phantom for 60° incident beam at various distance from phantom surface.

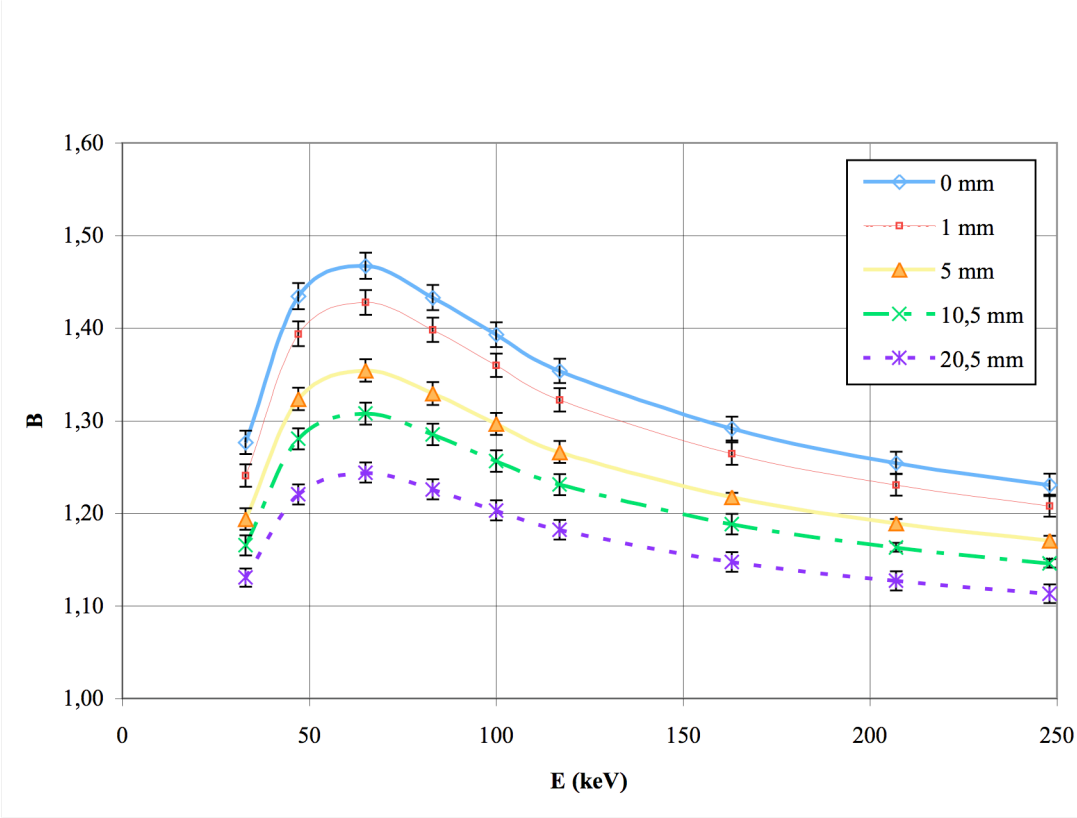

Figure D-5: Air kerma backscatter factors of the employed phantom for 75° incident beam at various distance from phantom surface.

Narrow spectrum series: 40 kV (E_{av} = 33 keV)
angular backscatter factor at varius distances
from the cylindrical phantom

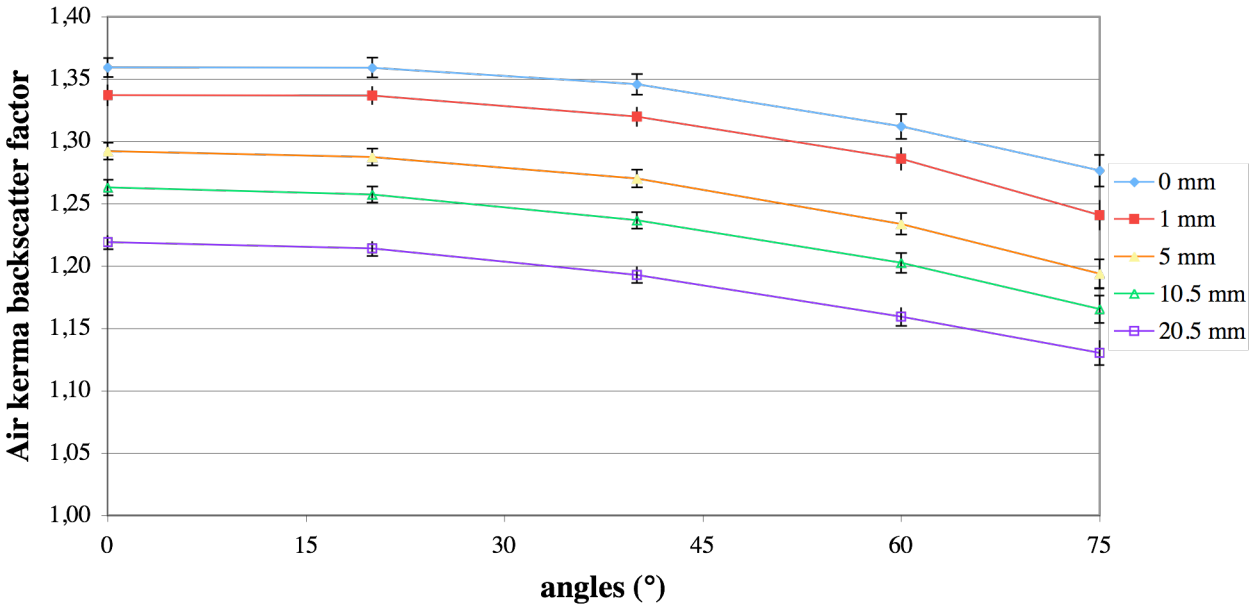

Narrow spectrum series: 60 kV (E_{av} = 47 keV)
angular backscatter factor at varius distances
from the cylindrical phantom

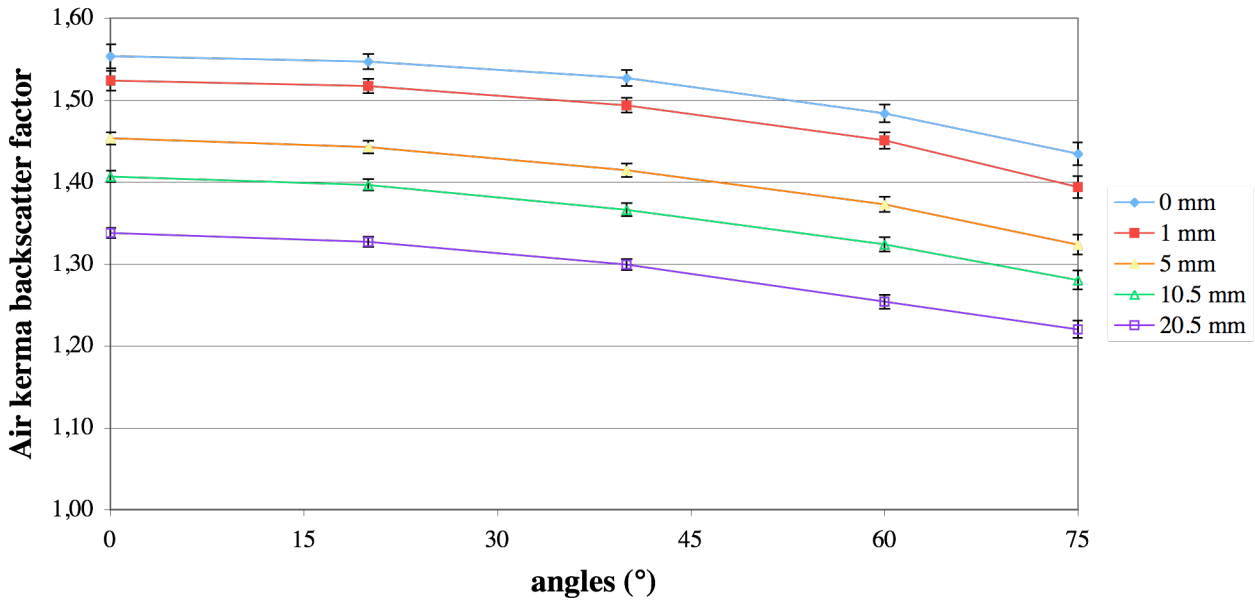

Narrow spectrum series: 80 kV (E_{av} = 65 keV)
angular backscatter factor at varius distances
from the cylindrical phantom

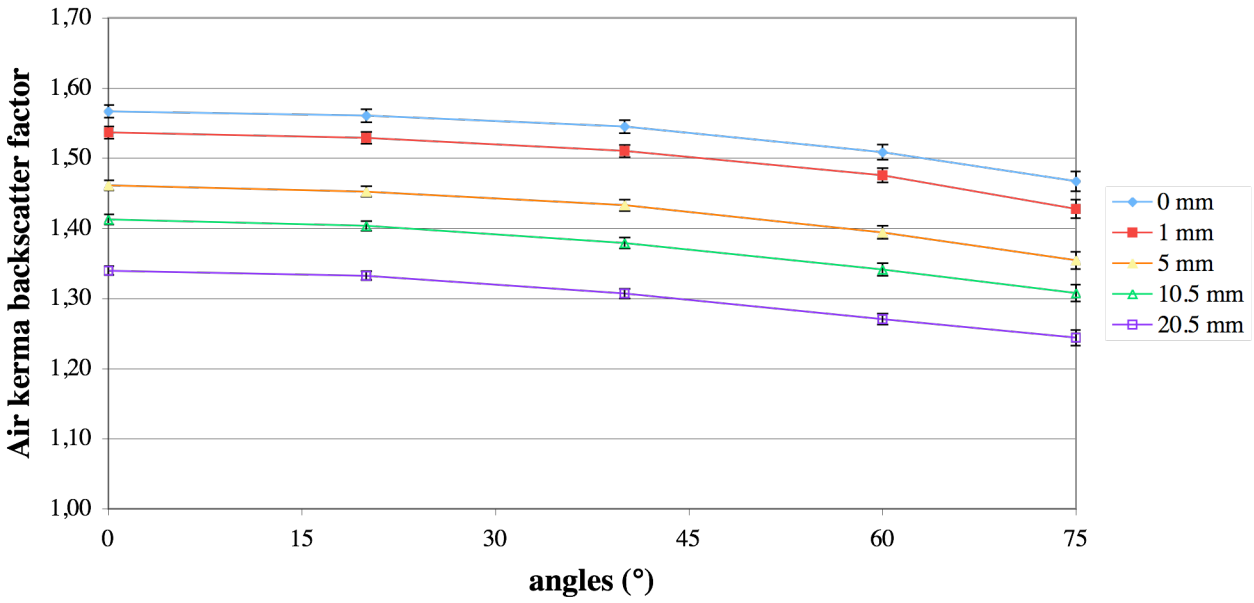

Narrow spectrum series: 100 kV (E_{av} = 83 keV)
angular backscatter factor at varius distances
from the cylindrical phantom

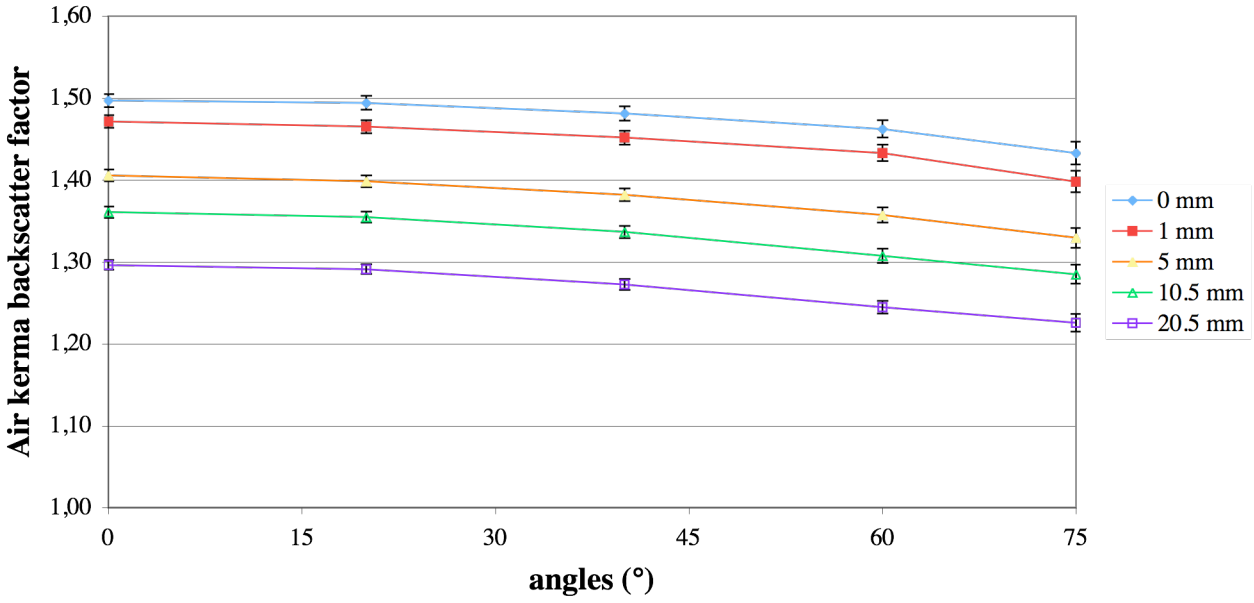

Narrow spectrum series: 120 kV (E_{av} = 100 keV)
angular backscatter factor at varius distances
from the cylindrical phantom

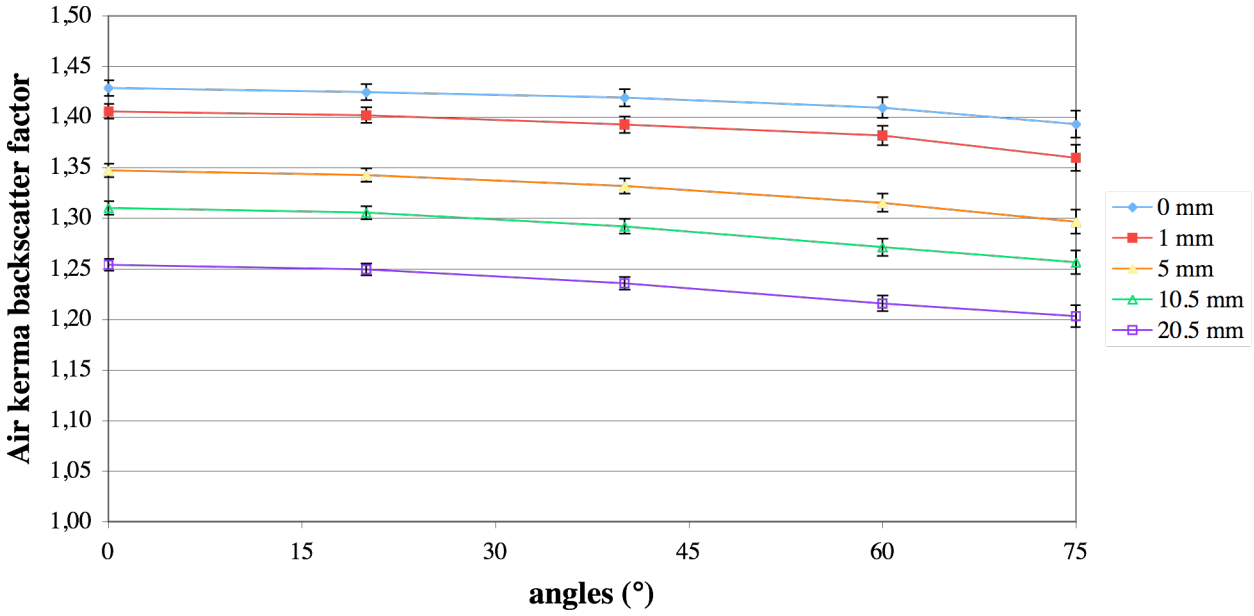

Narrow spectrum series: 150 kV (E_{av} = 117 keV)
angular backscatter factor at varius distances
from the cylindrical phantom

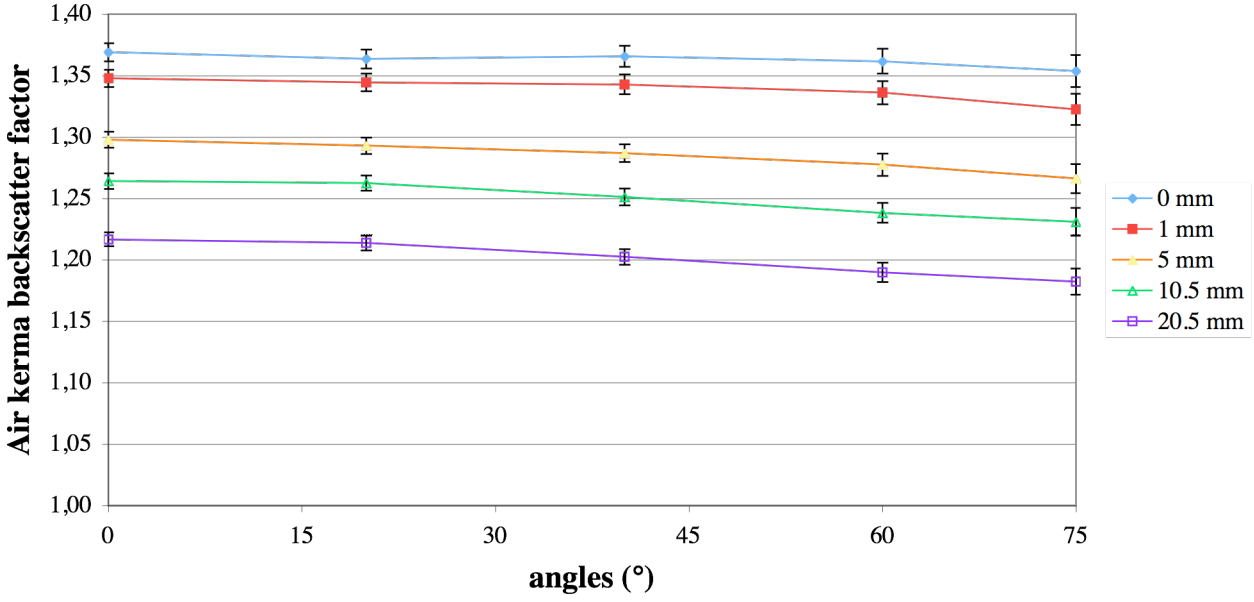

Narrow spectrum series: 200 kV (E_{av} = 163 keV)
angular backscatter factor at varius distances
from the cylindrical phantom

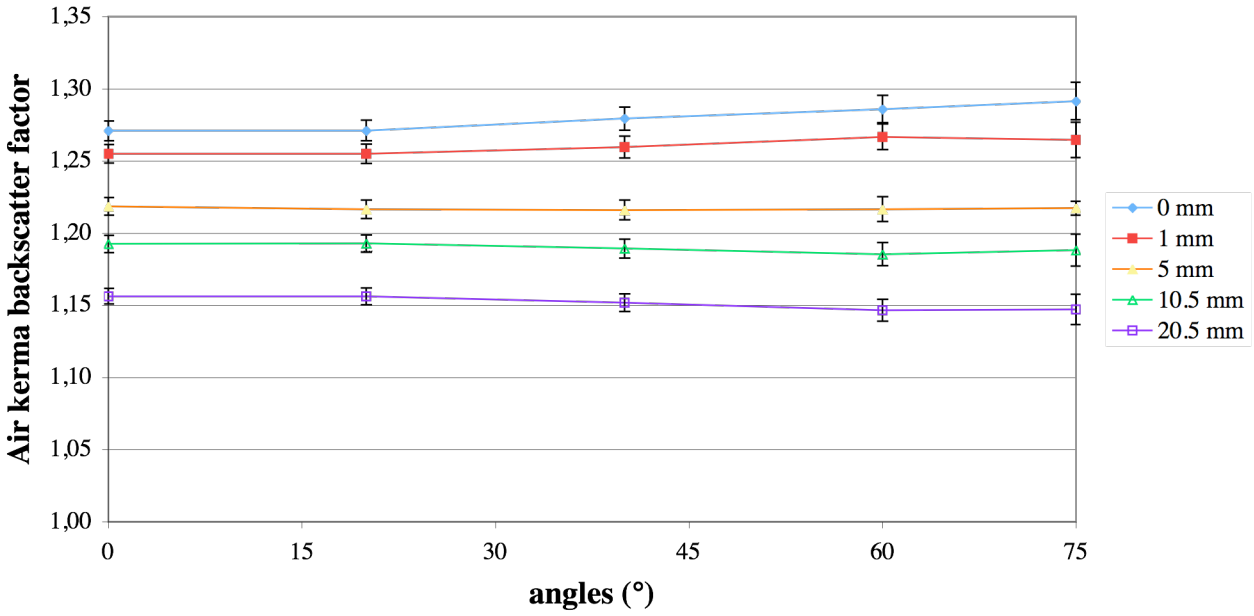

Narrow spectrum series: 250 kV (E_{av} = 207 keV)
angular backscatter factor at varius distances
from the cylindrical phantom

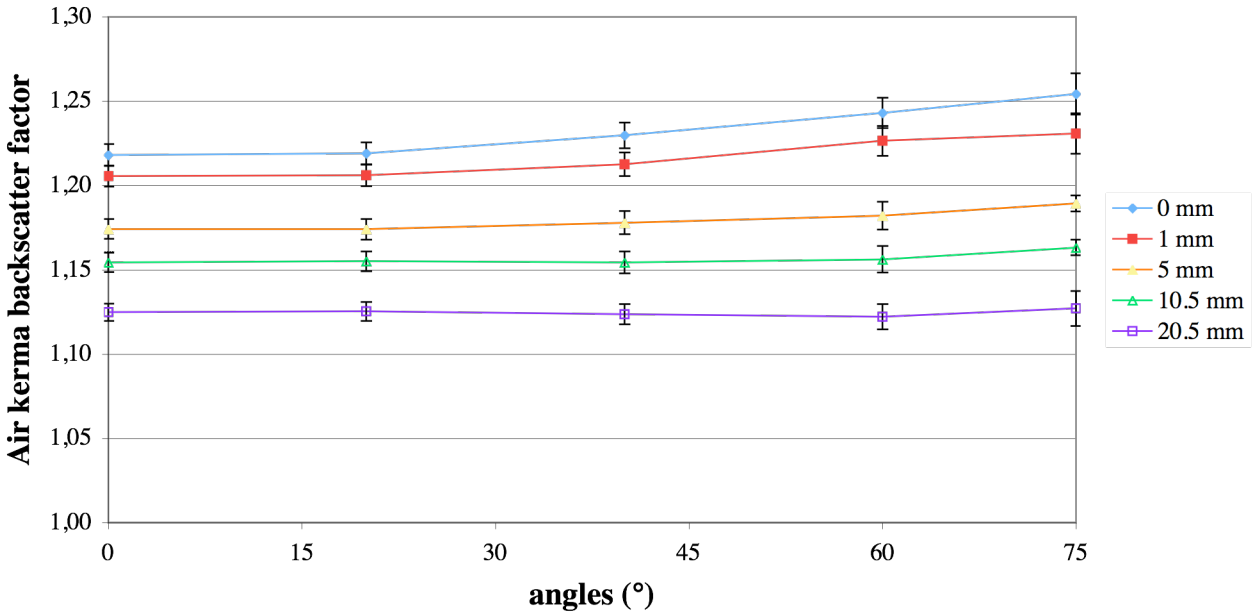

Narrow spectrum series: 300 kV (E_{av} = 248 keV)
angular backscatter factor at varius distances
from the cylindrical phantom

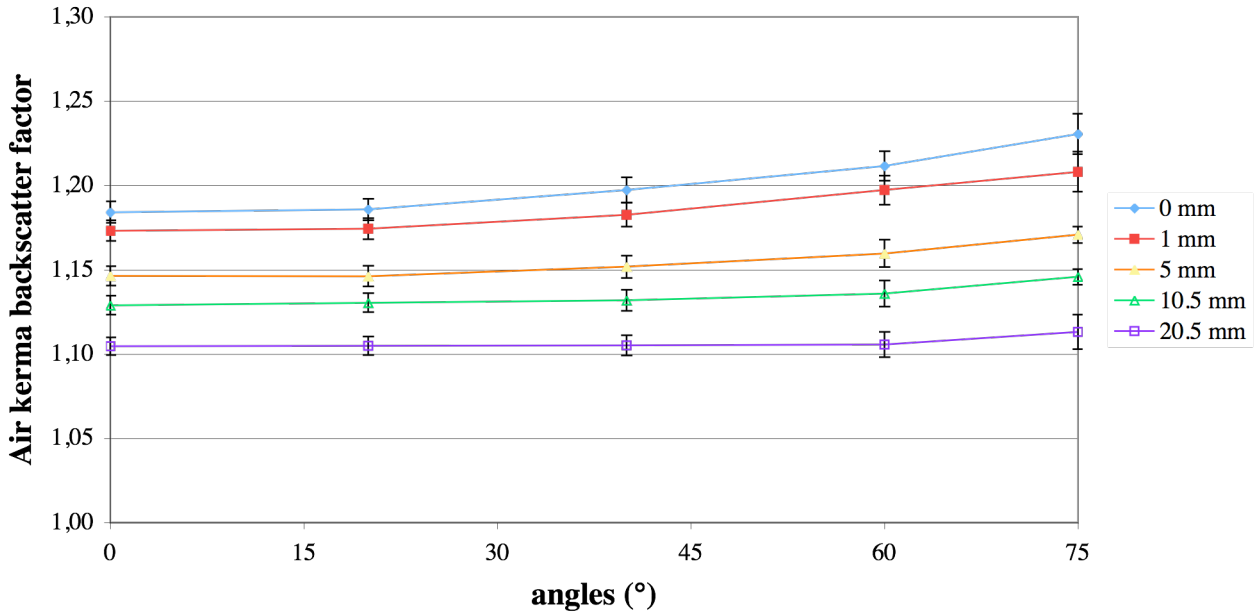

REFERENCES

[1] ORAMED Contract FP7 Grant Agreement 211361, Bruxelles 2008.

[2] International Commission on Radiological Protection, *The 2007 Recommendations of the International Commission on Radiological Protection,* ICRP Pubblication 103. Editor J. Valentin, Elsevier, London February 2008.

[3] Shore, R., *Cataract Risk after Low to Moderate Doses of Low-LET Radiation*, Winter school on low doses, EURADOS, PTB Braunschweig, 28th January 2009 to be published.

[4] Till, E., Zankl, M., Drexler, G., *Angular dependence of depth doses in a tissue slab irradiated with monoenergetic photons.* Neuherberg, Germany: GSF-National Research Centre for the Environment and Health; GSF-bericht 27/95 (1995).

[5] International Commission on Radiation Units and Measurements *Measurement of Dose Equivalents from External Photon and Electron Radiations*, ICRU Report 47. Bethesda – MD (USA) (1992).

[6] Ferrari, P., Gualdrini, G., Bedogni, R., Fantuzzi, E., Monteventi, F., Morelli, B., *Eye-Lens Dosimetry. A Critical Discussion on Hp(3) Operational Quantity*, ISSN/0393-3016, RT/2005/ION.

[7] International Commission on Radiation Units and Measurements *Conversion Coefficients for use in Radiological Protection Against External Radiation*, ICRU Report 51. Bethesda – MD (USA) (1998).

[8] International Organisation for Standardisation *Individual thermoluminescence dosemeters for extremities and eyes* ISO – 12974.

[9] Briesmeister, J.F.(Ed.) MCNP - *A General Monte Carlo N-Particle Transport Code*, Version 4C, Oak Ridge National Laboratory. LANL Manual LA-13709-M Version 4B Los Alamos (2000).

[10] Snyder, W.S., Ford, M.R., Warner, G.G. and Fisher, H.R., *Estimates of absorbed fraction for monoenergetic photon sources uniformly distributed in various organs of a heterogeneous phantom*, J. Nucl. Med. 10, S. 3, Pamphlet No. 5 (1969)

[11] International Organisation for Standardisation *X and gamma reference radiations for calibrating dosemeters and doserate meters and for determining their response as a function of photon energy.* BS ISO 4037-2 (1997).

Edito dall' ENEA
Funzione Centrale Relazioni Esterne
Unità Comunicazione
Lungotevere Thaon di Revel, 76 - 00196 Roma
www.enea.it
Stampa: Tecnografico ENEA - CR Frascati
Finito di stampare nel mese di febbraio 2009